Genome-edited powdery mildew resistance in wheat without growth penalties

https://doi.org/10.1038/s41586-022-04395-9

Received: 6 July 2021

Accepted: 20 December 2021

Published online: 9 February 2022

Check for updates

Shengnan Li[1,7], Dexing Lin[2,3,4,7], Yunwei Zhang[2,3,7], Min Deng[2,4,7], Yongxing Chen[2], Bin Lv[1,5], Boshu Li[2,3,4], Yuan Lei[2,3,4], Yanpeng Wang[2,3], Long Zhao[2,4], Yueting Liang[1,5], Jinxing Liu[2,3], Kunling Chen[2,3], Zhiyong Liu[2,4], Jun Xiao[2,4,6]✉, Jin-Long Qiu[1,5]✉ & Caixia Gao[2,3,4]✉

Disruption of susceptibility (*S*) genes in crops is an attractive breeding strategy for conferring disease resistance[1,2]. However, *S* genes are implicated in many essential biological functions and deletion of these genes typically results in undesired pleiotropic effects[1]. Loss-of-function mutations in one such *S* gene, *Mildew resistance locus O* (*MLO*), confers durable and broad-spectrum resistance to powdery mildew in various plant species[2,3]. However, *mlo*-associated resistance is also accompanied by growth penalties and yield losses[3,4], thereby limiting its widespread use in agriculture. Here we describe *Tamlo-R32*, a mutant with a 304-kilobase pair targeted deletion in the *MLO-B1* locus of wheat that retains crop growth and yields while conferring robust powdery mildew resistance. We show that this deletion results in an altered local chromatin landscape, leading to the ectopic activation of *Tonoplast monosaccharide transporter 3* (*TaTMT3B*), and that this activation alleviates growth and yield penalties associated with *MLO* disruption. Notably, the function of *TMT3* is conserved in other plant species such as *Arabidopsis thaliana*. Moreover, precision genome editing facilitates the rapid introduction of this *mlo* resistance allele (*Tamlo-R32)* into elite wheat varieties. This work demonstrates the ability to stack genetic changes to rescue growth defects caused by recessive alleles, which is critical for developing high-yielding crop varieties with robust and durable disease resistance.

Plant diseases cause losses of 11–30% in crop production per year worldwide, threatening global food security[5]. Molecular breeding is an effective and sustainable strategy to improve plant disease resistance[6]. Dominant resistance (*R*) genes are frequently adopted for breeding resistance against a specific pathogen[7–9]. Most *R* genes encode nucleotide-binding site–leucine-rich-repeat proteins that directly or indirectly recognize pathogenic effector proteins and trigger immunity[10,11]. *R* gene-mediated resistance is race-specific, and pathogens can readily overcome the resistance by introducing escape mutations in their respective effector genes[12]. Disruption of *S* genes is thus an attractive alternative for resistance breeding in crops[1,3,13].

S genes are plant genes that are leveraged by pathogens to achieve successful infection[14]. Disease resistance conferred by *S* gene mutations is genetically recessive and non-race-specific[1,15,16]. *MLO* is a well-characterized *S* gene[3,17,18]. There are more than 650 species of powdery mildew fungi that infect about 10,000 plant species[19]. Loss-of-function mutations in *MLO* result in durable and broad-spectrum resistance to powdery mildew[2–4,20,21]. However, *mlo* mutations generally lead to substantial growth penalties. In barley and *Arabidopsis*, loss-of-function *mlo* mutants are associated with spontaneous callose deposition, cell death and early senescence[3,4,22,23]. Therefore, only weak *mlo* alleles with balanced resistance and growth phenotypes, such as *mlo*-11 in barley, have been used to breed elite varieties[23,24]. Although *mlo* resistance is conserved across plant species[19,25], the growth trade-offs have prevented its wide deployment in agriculture.

Wheat (*Triticum aestivum*) is a major staple crop around the world. Powdery mildew disease seriously threatens wheat yields, which must increase to meet the demands of an expanding global population[26]. We previously generated a wheat *mlo* mutant, *Tamlo-aabbdd*, using genome editing to simultaneously knock out all three homeologues of *TaMLO1* in Kenong 199 wheat[20]. Although this wheat mutant exhibited robust and broad-spectrum resistance to powdery mildew, it was affected by undesired pleiotropic effects such as accelerated senescence[27]. Here we describe *Tamlo-R32*, a wheat *mlo* mutant that confers robust disease resistance without undesirable pleiotropic effects.

Tamlo-R32 is resistant with no growth defect

Although the *Tamlo-aabbdd* mutant wheat plants were highly resistant to powdery mildew (*Blumeria graminis* f. sp. *tritici, Bgt*) (Fig. 1a, b), they exhibited defects in both plant height and grain yield compared with wild-type plants (Fig. 1c–e).

[1]State Key Laboratory of Plant Genomics, Institute of Microbiology, Innovation Academy for Seed Design, Chinese Academy of Sciences, Beijing, China. [2]State Key Laboratory of Plant Cell and Chromosome Engineering, Institute of Genetics and Developmental Biology, Innovation Academy for Seed Design, Chinese Academy of Sciences, Beijing, China. [3]Center for Genome Editing, Institute of Genetics and Developmental Biology, Chinese Academy of Sciences, Beijing, China. [4]College of Advanced Agricultural Sciences, University of Chinese Academy of Sciences, Beijing, China. [5]CAS Center for Excellence in Biotic Interactions, University of Chinese Academy of Sciences, Beijing, China. [6]CAS-JIC Centre of Excellence for Plant and Microbial Science, Institute of Genetics and Developmental Biology, Chinese Academy of Sciences, Beijing, China. [7]These authors contributed equally: Shengnan Li, Dexing Lin, Yunwei Zhang, Min Deng. ✉e-mail: jxiao@genetics.ac.cn; qiujl@im.ac.cn; cxgao@genetics.ac.cn

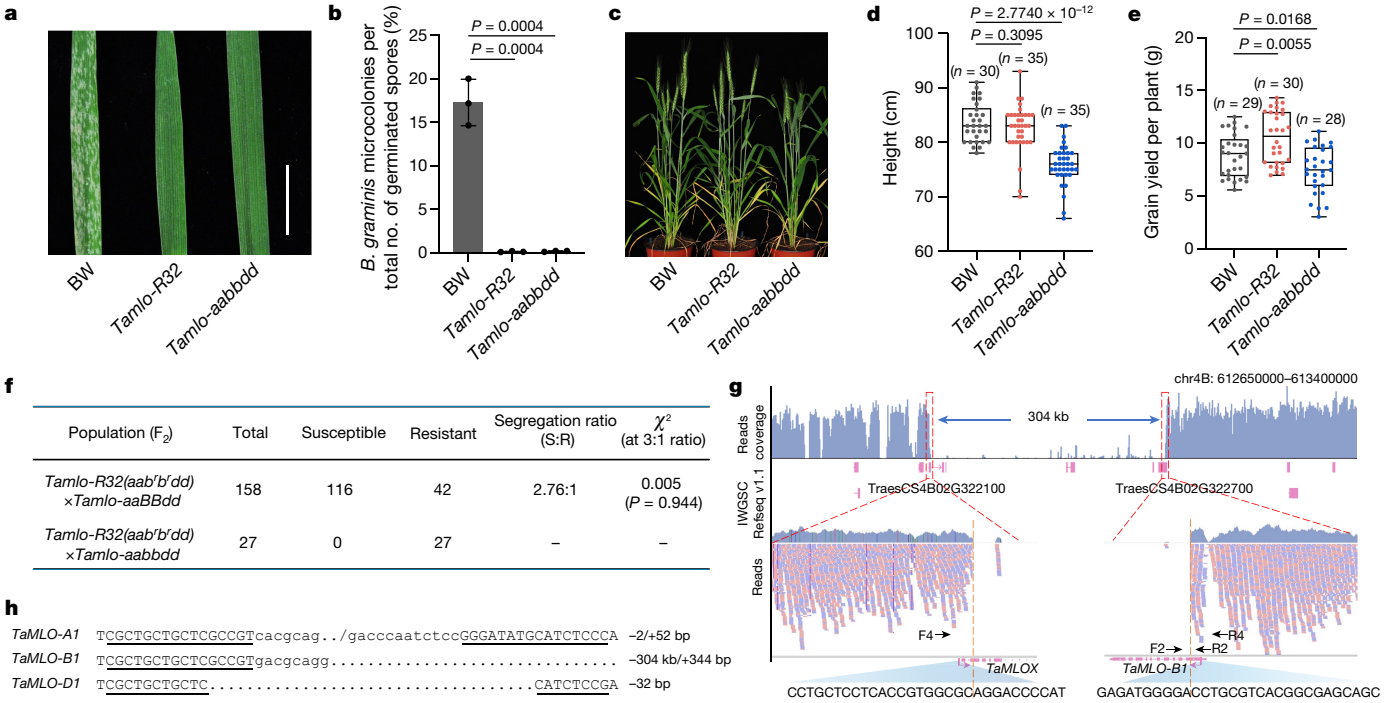

Fig. 1 | *Tamlo-R32* wheat exhibits immunity to powdery mildew without growth and yield penalties. a, Macroscopic infection phenotype of representative detached wheat leaves of the indicated genotypes in the Bobwhite background (BW) with *Bgt* isolate E09. Scale bar, 1 cm. **b**, Percentages of microcolonies formed from the total number of *Bgt* germinated spores on the leaves of the indicated plants. Data are mean ± s.d. ($n = 3$). Two-tailed Student's *t*-tests. **c**, Morphology of the indicated wheat plants grown in a growth room. **d**, **e**, Plant height (**d**) and grain yield per plant (**e**) of the indicated plants. Plants were grown in field conditions in Beijing. *n* represents the sample size. Two-tailed Mann–Whitney tests or two-tailed Student's *t*-tests. In box plots, the box limits indicate the 25th and 75th percentiles, the whiskers indicate the full range of the data, and the centre line indicates the median. Individual data points are plotted. **f**, Genetic crosses to pinpoint the *Tamlo-R32* mutation. The genotype of the *Tamlo-R32* mutant is assumed to be *aab'b'dd*. **g**, Next-generation sequencing uncovers a 304,374 bp deletion on chromosome 4B of *Tamlo-R32*. Red dotted rectangles indicate the ends of the deletion. Black arrows denote the position and orientation of the F2–R2 and F4–R4 primer pairs used in Extended Data Fig. 1d. **h**, Genotype of *Tamlo-R32*. Underlines indicate the TALEN targeting sequences. Detailed sequence information is available in Extended Data Fig. 1e.

When generating additional wheat *mlo* mutants using the TALEN vector[20,28], we identified the *Tamlo-R32* mutant in the Bobwhite background in a T_1 population. We first evaluated the resistance phenotype of this mutant after establishing that it was transgene-free (Extended Data Fig. 1a). Similar to the *Tamlo-aabbdd* mutant, *Tamlo-R32* exhibited robust resistance to powdery mildew (Fig. 1a). Microscopic examination revealed a marked reduction in the number of microcolonies formed on *Tamlo-R32* leaves (Fig. 1b). Notably, the *Tamlo-R32* mutant displayed no growth penalties in terms of plant height and grain yield when grown in the field (Fig. 1c–e, Extended Data Fig. 2a–d).

Tamlo-R32 harbours a 304-kb deletion

The *Tamlo-R32* mutant was generated using a TALEN vector that targets all three wheat *MLO1* genes. We initiated mutant genotyping by selectively amplifying targeted fragments of *TaMLO-A1*, *TaMLO-B1* and *TaMLO-D1* using gene-specific primer pairs (Extended Data Fig. 1b). Although we successfully amplified all three genes from the wild-type plant, we could not amplify *TaMLO-B1* from *Tamlo-R32* (Extended Data Fig. 1c). This suggested that there was a substantial perturbation in the B genome of *Tamlo-R32*.

We performed genetic crosses to pinpoint the mutations involved in *Tamlo-R32* resistance. We used the *Tamlo-R32* mutant as the maternal line and crossed it with two different paternal lines. One of these, *Tamlo-aaBBdd*, was susceptible to powdery mildew, whereas the other, *Tamlo-aabbdd*, was resistant. We subsequently evaluated the F_2 progenies of these crosses for resistance to powdery mildew. In the *Tamlo-R32* × *Tamlo-aaBBdd* F_2 population, 116 plants were susceptible and 42 plants were resistant, fitting a segregation ratio of 3:1. All 27 F_2 plants from the *Tamlo-R32* × *Tamlo-aabbdd* cross were resistant to powdery mildew disease. These results indicate that the resistance allele in *Tamlo-R32* is tightly linked to the *TaMLO-B1* locus (Fig. 1f, Extended Data Fig. 3a, b).

We next performed whole-genome sequencing to precisely genotype *Tamlo-R32*. After aligning the sequencing reads with the Chinese Spring wheat reference genome (IWGSC, Refseq v1.1), we identified a 304-kilobase pair large deletion (from position 612856038 to 613160412) on chromosome 4B of *Tamlo-R32*. The right boundary of the deletion was located in the second exon of *TaMLO-B1*, and the left boundary terminated in an *MLO*-like gene (hereafter referred to as *TaMLOX*) (Fig. 1g). Targeted PCR amplification and sequencing of genomic DNA confirmed this large deletion in *Tamlo-R32* (Fig. 1h, Extended Data Fig. 1d, e).

TaTMT3B is upregulated in *Tamlo-R32*

To investigate the effect of this large deletion, we performed RNA sequencing (RNA-seq) using 7-day-old leaf tissues of *Tamlo-R32* and wild-type Bobwhite and examined the expression of genes within an 8-Mb region upstream and downstream of the deletion. As expected, expression of genes located within the deleted region was either undetectable or downregulated. These genes are either functionally dispensable, as suggested by the overall expression levels in different tissues, or functionally redundant with homeologues on the A and D genomes owing to similar expression patterns, abundance and protein products[29] (Extended Data Fig. 4a–c). Of note, *TraesCS4B02G322000*, a gene located immediately upstream of the deletion, was markedly

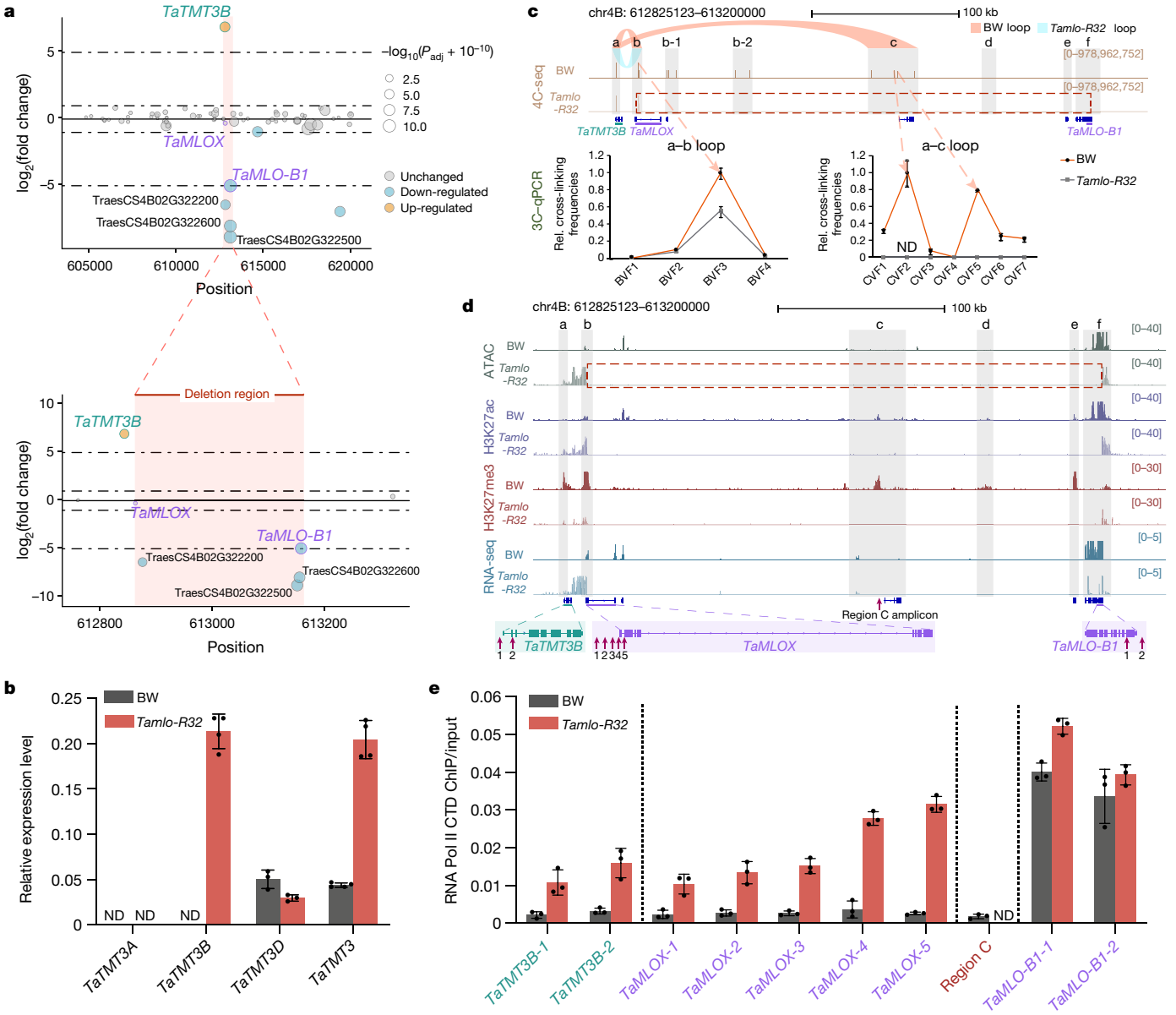

Fig. 2 | Chromosomal rearrangement in *Tamlo-R32* leads to activation of *TaTMT3B* in leaves. a, Differentially expressed genes around the *TaMLO-B1* locus in *Tamlo-R32*. Each circle represents one gene, with size indicating statistical significance (adjusted *P* value (P_{adj})) and colour representing different expression categories, as indicated. Differentially expressed genes were called by the R package edgeR with a threshold absolute value of $\log_2$(fold change) ≥1 and adjusted *P* value (false discovery rate method) ≤0.05. RNA-seq was performed on 7-day-old plant leaves. **b**, Expression levels of *TaTMT3A*, *TaTMT3B*, *TaTMT3D* and total *TaTMT3* in leaves of Bobwhite and *Tamlo-R32* plants. Data are normalized to the *TaPARG* gene. Data are mean ± s.d. (*TaTMT3A*, *TaTMT3B* and *TaTMT3* in Bobwhite and *Tamlo-R32*: $n = 4$; *TaTMT3D* in Bobwhite and *Tamlo-R32*: $n = 3$). **c**, Detection of chromatin loops between the *TaTMT3B* promoter and intergenic regions within *TaMLOX* and *TaMLO-B1*. 4C-seq was used for initial screening of loops linked to the *TaTMT3B* promoter (top); 3C with quantitative PCR was used for validation and quantification of the a–b and a–c loops (bottom). Rel., relative. **d**, Chromatin accessibility, H3K27me3, H3K27ac and transcription profiles in the *TaTMT3B-MLO-B1* region of Bobwhite and *Tamlo-R32*, visualized by Integrative Genomics Viewer. Red dotted rectangles indicate the large region deletion in *Tamlo-R32* in **c**, **d**. **e**, Transcriptional activity in the *TaTMT3B-MLO-B1* region in Bobwhite and *Tamlo-R32* plants. The locations of individual PCR amplicons are shown by arrows in **d**. Data are mean ± s.d. ($n = 3$). ND, not detected.

upregulated in *Tamlo-R32* relative to wild-type Bobwhite (Fig. 2a). This gene (hereafter referred to as *TaTMT3B*) is an orthologue[30] of *Arabidopsis AtTMT3*. Upregulation of *TaTMT3B* was further validated by quantitative PCR with reverse transcription (RT–PCR), whereas the expression of a further 19 nearby genes was unchanged (Extended Data Fig. 5a, b). There are three homeologues of *TaTMT3*—namely *TaTMT3A*, *TaTMT3B* and *TaTMT3D*—and only *TaTMT3B* was upregulated in the *Tamlo-R32* mutant, leading to increased total levels of *TaTMT3* (Fig. 2b). *TaTMT3* genes are silenced in all tissues evaluated in wild-type wheat except in the spike[29] (Extended Data Fig. 4a, d).

To explore mechanisms regulating *TaTMT3B* expression, we examined histone modifications and chromatin accessibility in the *TaTMT3B-MLO-B1* region by performing cleavage under targets and tagmentation (CUT&Tag) and assay for transposase-accessible chromatin sequencing (ATAC-seq) using leaf tissues. In wild-type wheat, H3K27me3—which is involved in the formation of long-range chromatin loops leading to gene silencing[31]—marks genes that are expressed at low levels, including *TaTMT3B*, *TaMLOX* and other distal genes (Extended Data Fig. 4e). We next performed chromosome conformation capture sequencing (3C-seq) and circular 3C-seq (4C-seq) and found that

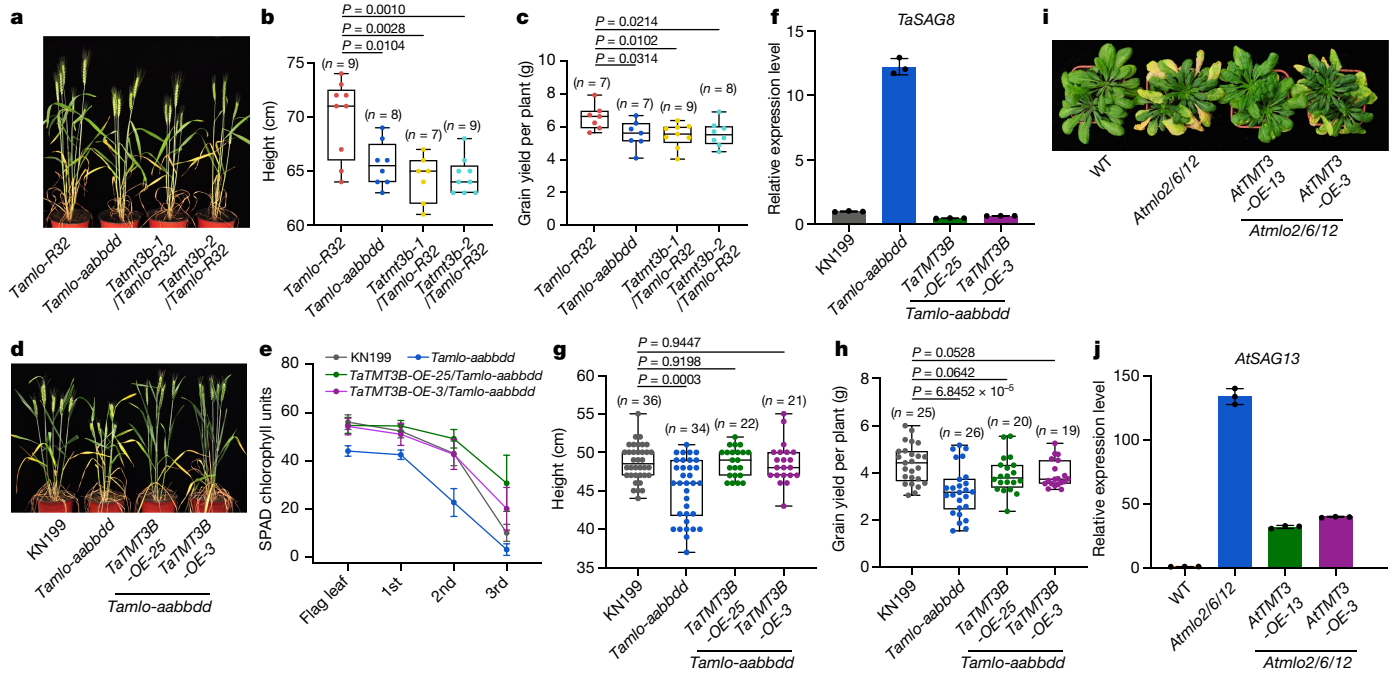

Fig. 3 | Increased *TMT3* expression rescues growth phenotypes in *mlo* mutants of wheat and *Arabidopsis*. **a**–**c**, Knockout of *TaTMT3B* in *Tamlo-R32* worsens growth phenotypes (**a**), plant height (**b**) and grain yield per plant (**c**). Wheat plants in **a**–**c** were all Bobwhite. **d**–**h**, Overexpression of *TaTMT3B* (OE) in the *Tamlo-aabbdd* mutant rescues growth phenotypes (**d**). **e**, Relative Soil Plant Analysis Development (SPAD) chlorophyll units in flag, 1st, 2nd and 3rd leaves of KN199 (n = 14, 16, 14 and 6, respectively), *Tamlo-aabbdd* (n = 13, 11, 10 and 6, respectively), *TaTMT3B-OE-25/Tamlo-aabbdd* (n = 22, 18, 18 and 19, respectively) and of *TaTMT3B-OE-3/Tamlo-aabbdd* (n = 15, 13, 18 and 11, respectively). **f**, Relative expression levels of *TaSAG8* in wheat leaves. Results are normalized to *TaACTIN*, and the *TaSAG8* expression level in KN199 was set to 1 (n = 3). Samples were collected at the heading stage from the second leaf below the flag leaf. **g**, **h**, Plant height (**g**) and grain yield per plant (**h**) of wheat plants measured at the mature stage. Wheat plants in **d**–**h** were all KN199. Wheat in **a**–**h** were grown in a growth room. **i**, Senescence phenotypes in *Arabidopsis* plants of indicated genotypes. Plants were grown for 8 weeks under short-day conditions. **j**, Relative expression levels of *AtSAG13* in *Arabidopsis* leaves of the indicated genotypes. Results are normalized to *Arabidopsis AtACTIN8*, and the *AtSAG13* expression level in WT was set to 1 (n = 3). Plants were grown under short-day conditions for seven weeks after sowing, and rosette leaf seven of each plant was sampled. In box plots in **b**, **c**, **g**, **h**, the box limits indicate the 25th and 75th percentiles, whiskers indicate the full range of the data, and the centre line indicates the median. Individual data points are plotted. n represents sample size. All data are mean ± s.d. Two-tailed Mann–Whitney tests or two-tailed Student's t-tests.

the H3K27me3-marked promoter of *TaTMT3B* in wild-type Bobwhite was indeed looped with distal loci marked by H3K27me3 within the *TaTMT3B-MLO-B1* regions (Fig. 2c). By contrast, H3K27me3 levels were low in the highly expressed *TaMLO-B1* locus, which was in an accessible chromatin region (Extended Data Fig. 4e).

We reasoned that the 304-kb deletion in *Tamlo-R32* might alter local chromatin states and in turn affect gene expression. In agreement, the large deletion abolished chromatin looping between the *TaTMT3B* promoter and a region within the deletion (a–c loop) (Fig. 2c, d). Consistently, we also detected a substantial loss of H3K27me3 signal and a marked increase in both ATAC-seq and H3K27ac signals at the *TaTMT3B* and *TaMLOX* regions in *Tamlo-R32*, along with an increased abundance of transcripts (Fig. 2d). Moreover, active RNA polymerase II (Pol II CTD-S5p) deposition was increased in the *TaTMT3B* locus and *TaMLOX* region in the *Tamlo-R32* mutant (Fig. 2e). Meanwhile, strong Pol II CTD-S5p deposition was observed at the *TaMLO-B1* promoter in both wild-type and *Tamlo-R32* plants (Fig. 2e). These data suggest that transcription of *TaTMT3B* is repressed by the presence of the repressive histone mark H3K27me3 and inhibitory chromatin loops in wild-type Bobwhite, whereas the large deletion in *Tamlo-R32* abolishes the epigenetic repression and creates a permissive chromatin environment around *TaTMT3B* (Extended Data Fig. 4f).

TaTMT3B overexpression rescues penalties

To confirm that the phenotypes observed in the *Tamlo-R32* mutant were a result of *TaTMT3B* upregulation, we used CRISPR–Cas9 to knock out *TaTMT3B* in *Tamlo-R32* (Extended Data Fig. 6a). The resulting *Tatmt3b/Tamlo-R32* plants resumed undesirable phenotypes of reduced plant height and yield losses (Fig. 3a–c). Therefore, *TaTMT3B* was critical for rescuing the growth defects caused by *TaMLO1* knockout.

To further validate its function, *TaTMT3B* was overexpressed in a *Tamlo-aabbdd* mutant of Kenong 199 (KN199). Whereas the KN199 *Tamlo-aabbdd* mutant exhibited accelerated leaf senescence at the heading stage[27] (Fig. 3d), the *TaTMT3B*-overexpressing derivatives maintained normal phenotypes (Fig. 3d, Extended Data Fig. 6b). Consistent with this, relative chlorophyll content was significantly reduced in the leaves of the *Tamlo-aabbdd* mutant, but was recovered in the two *TaTMT3B*-overexpressing lines (Fig. 3e). Since leaf senescence is often accompanied by an increased expression of senescence-associated genes (SAGs), we measured the expression of *TaSAG8* (ref. [32]). *TaSAG8* transcript levels were increased in *Tamlo-aabbdd* mutant leaves, but normalized following *TaTMT3B* overexpression (Fig. 3f). Notably, the reduced plant height and grain yield losses caused by the *mlo* triple knockout were also rescued by *TaTMT3B* overexpression without compromising powdery mildew resistance (Fig. 3g, h, Extended Data Fig. 6c–e).

TMT3 function is conserved in *A. thaliana*

Since *mlo*-associated resistance to powdery mildew is evolutionarily conserved across plant species[19,25], we set out to test whether the function of *TMT3* is also conserved in other plant species.

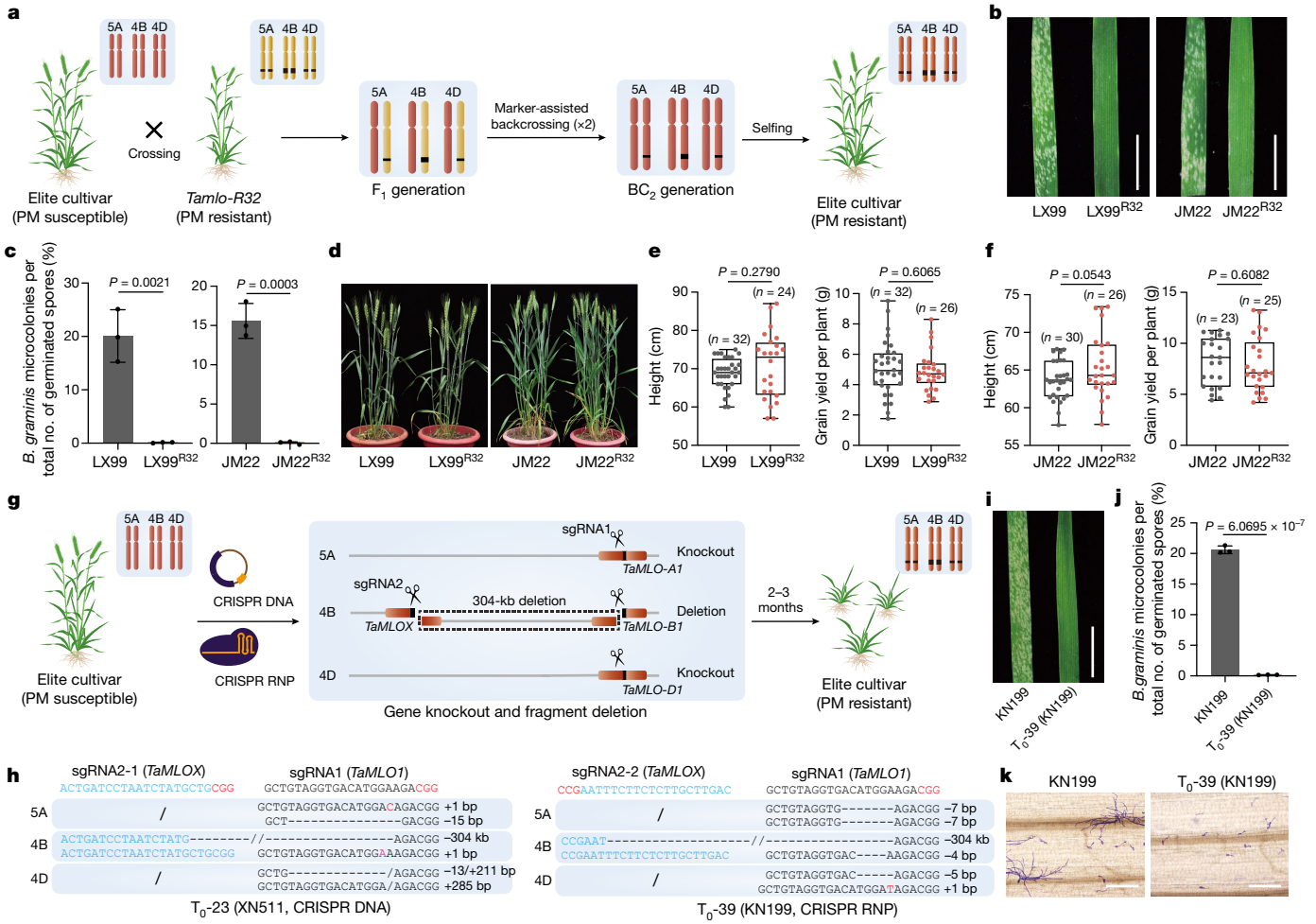

Fig. 4 | Introduction of the *Tamlo-R32* allele into elite wheat varieties. **a**, Scheme for developing new wheat germplasms harboring the *Tamlo-R32* allele by marker-assisted backcrossing. **b**, **i**, Macroscopic infection phenotypes of the novel wheat germplasms using marker-assisted backcrossing (**b**) or CRISPR–Cas9 RNP (**i**) seven days after inoculation with *Bgt* isolate GH5 (**b**) or E09 (**i**). Scale bar, 1 cm. **c**, **j**, Percentage of microcolonies formed from the total number of germinated spores of *Bgt* on leaves of the new wheat germplasms using marker-assisted backcrossing (**c**) or CRISPR–Cas9 RNP (**j**). Data are mean ± s.d. ($n = 3$). Two-tailed Mann–Whitney tests or two-tailed Student's *t*-tests. **d**, Growth phenotype of indicated wheat plants grown under field conditions. **e**, **f**, Plant height and grain yield per plant of LX99 and LX99^{R32} (**e**) or JM22 and JM22^{R32} (**f**). Plants were grown in a greenhouse. *n* represents the sample size. In box plots in **e**, **f**, the box limits indicate the 25th and 75th percentiles, whiskers indicate the full range of the data, and the centre line indicates the median. Individual data points are plotted. Two-tailed Mann–Whitney tests or two-tailed Student's *t*-tests. **g**, Schematic of rapid introduction of the *Tamlo-R32* allele into elite wheat varieties using CRISPR–Cas9 DNA or RNP with only two sgRNAs. PM, powdery mildew. **h**, Genotypes of two of the mutants generated by CRISPR–Cas9 DNA and RNP technologies. sgRNA1 targets all three *MLO1* homeologues; sgRNA2 targets the B genome *MLOX* specifically. **k**, Micrographs of microcolony formation by *Bgt* on wheat leaves of the indicated genotypes. Scale bars, 100 µm.

We first overexpressed *AtTMT3* in an *A. thaliana Atmlo2/6/12* mutant[4]. *AtTMT3* overexpression largely rescued premature leaf senescence in an *Atmlo2/6/12* mutant (Fig. 3i, Extended Data Fig. 6f–h). Accordingly, the transcript level of the senescence marker gene[33] *AtSAG13* was greatly reduced in the *Atmlo2/6/12* mutant overexpressing *AtTMT3* (Fig. 3j). Resistance to powdery mildew in the *Atmlo2/6/12* mutant was not compromised by overexpressing *AtTMT3* (Extended Data Fig. 6i–k). These results indicate a conserved function of *TMT3* in *A. thaliana*.

Programmed genome editing in elite wheat

There is a global need for elite wheat varieties with robust powdery mildew resistance and no yield loss. We first attempted to introgress the superior *Tamlo-R32* alleles from the Bobwhite background into two elite Chinese wheat varieties, Liangxing99 (LX99) and Jimai22 (JM22) (Fig. 4a). We obtained both LX99 and JM22 with these *Tamlo-R32* alleles (LX99^{R32} and JM22^{R32}, respectively) from the BC_2F_3 population, and found that both variants exhibited strong resistance to powdery mildew (Fig. 4b, c). As expected, they also had normal growth phenotypes and grain yields similar to the wild-type recurrent parent (Fig. 4d–f). However, the process of introgression is laborious and time consuming.

Genome editing is rapidly revolutionizing plant breeding[34]. We applied CRISPR–Cas9 to develop new wheat germplasms harbouring the *Tamlo-R32* allele. We used only one pair of single guide RNAs (sgRNAs) to achieve simultaneous editing of all three *TaMLO1* genes and the desired large deletion in the wheat B genome (Fig. 4g). We targeted sgRNA1 to a site conserved in all three *TaMLO1* homeologues, and targeted sgRNA2 to *TaMLOX* specifically in the B genome. Constructs expressing the two sgRNAs and *Streptococcus pyogenes* Cas9 were co-delivered by particle bombardment into immature embryos of KN199, Xinong511 (XN511), Shi4185 (S4185) and Xiaoyan60 (XY60), four elite winter wheat varieties grown in China. Under selection-free condition, we recovered a total of 15 (KN199), 12 (XN511), 2 (S4185) and 2 (XY60) T_0 mutants containing the programmed large deletion in the B genome, with efficiencies of 0.9%, 0.9%, 0.4% and 0.3%, respectively (Extended Data Table 1). Among these mutants, 5 KN199 (33.3%), 7 XN511

(58.3%) and 2 S4185 (100%) mutants also contained site-specific indels in at least one allele in both *MLO-A1* and *MLO-D1* (Fig. 4h, Extended Data Tables 1, 2). Since transient expression of CRISPR–Cas9 DNA followed by selection-free regeneration can greatly reduce transgene integration[35], we found that more than one-third of the mutants we obtained in the T_0 generation displayed no transgene integration (Extended Data Fig. 7, Extended Data Table 2).

We next performed targeted editing using CRISPR–Cas9 ribonucleoproteins (RNPs) to completely eliminate transgene integration and small DNA insertions in the generated mutants[36]. RNP was delivered into immature embryos of KN199, S4185 and XY60 by particle bombardment. The desired 304-kb deletion mutants were obtained at frequencies of 0.7% (KN199), 0.4% (S4185) and 0.2% (XY60), respectively. Two (50%) of the mutants in KN199 also contained indels in at least one allele in both *MLO-A1* and *MLO-D1* (Fig. 4g, Extended Data Tables 1, 3). The T_0-39 mutant was challenged with powdery mildew, and exhibited resistance similar to *Tamlo-R32* (Fig. 4i–k). These findings highlight genome editing as a powerful strategy to introduce the *Tamlo-R32* alleles into elite wheat varieties.

Discussion

In this study, we found that the wheat *Tamlo-R32* mutant harbours a chromosomal rearrangement in the wheat B genome, and through epigenetic changes, results in a significant upregulation of *TaTMT3B* expression. We demonstrated that this alteration counteracts the negative penalties associated with *mlo* mutations while maintaining robust disease resistance. Therefore, the *Tamlo-R32* variant is an attractive starting point for breeding powdery mildew-resistant wheat without growth and yield penalties. We also demonstrated that genome editing can facilitate the engineering of *Tamlo-R32* alleles into elite wheat varieties.

Although further work is needed to elucidate *TMT3* function, it is beneficial to engage this *Tamlo-R32* mutant in wheat breeding. We also describe the use of CRISPR–Cas9 to precisely edit the *MLO* locus in four elite winter wheat varieties. The function of *TMT3* appears to be conserved across different plant species, suggesting wide applicability among crop species. In sum, our work represents an important step towards the expansion of *mlo*-associated resistance across agriculture.

S gene-mediated recessive disease resistance is frequently accompanied by growth defects and yield losses in crops, preventing its deployment in food production. Previous attempts have been ineffective at alleviating these undesired pleiotropic effects[4,19,37]. This Article describes a host gain-of-function mutation that overcomes the growth defects caused by recessive resistance alleles. We anticipate that similar mutations will be identified in other *S* genes that confer *S* gene-mediated disease resistance without undesired pleiotropic effects. The application of sophisticated genome-editing technologies promises to support the development of sustainable disease-resistant crops that satisfy future needs.

Online content

Any methods, additional references, Nature Research reporting summaries, source data, extended data, supplementary information, acknowledgements, peer review information; details of author contributions and competing interests; and statements of data and code availability are available at https://doi.org/10.1038/s41586-022-04395-9.

1. van Schie, C. C. & Takken, F. L. Susceptibility genes 101: how to be a good host. *Annu. Rev. Phytopathol.* **52**, 551–581 (2014).
2. Schulze-Lefert, P. & Vogel, J. Closing the ranks to attack by powdery mildew. *Trends Plant Sci.* **5**, 343–348 (2000).
3. Büschges, R. et al. The barley *Mlo* gene: a novel control element of plant pathogen resistance. *Cell* **88**, 695–705 (1997).
4. Consonni, C. et al. Conserved requirement for a plant host cell protein in powdery mildew pathogenesis. *Nat. Genet.* **38**, 716–720 (2006).
5. van Esse, H. P., Reuber, T. L. & van der Does, D. Genetic modification to improve disease resistance in crops. *New Phytol.* **225**, 70–86 (2020).
6. Li, W., Deng, Y., Ning, Y., He, Z. & Wang, G.-L. Exploiting broad-spectrum disease resistance in crops: from molecular dissection to breeding. *Annu. Rev. Plant Biol.* **71**, 575–603 (2020).
7. Dangl, J. L., Horvath, D. M. & Staskawicz, B. J. Pivoting the plant immune system from dissection to deployment. *Science* **341**, 746–751 (2013).
8. Deng, Y. et al. Epigenetic regulation of antagonistic receptors confers rice blast resistance with yield balance. *Science* **355**, 962–965 (2017).
9. Saintenac, C. et al. Wheat receptor-kinase-like protein Stb6 controls gene-for-gene resistance to fungal pathogen *Zymoseptoria tritici*. *Nat. Genet.* **50**, 368–374 (2018).
10. Jones, J. D. & Dangl, J. L. The plant immune system. *Nature* **444**, 323–329 (2006).
11. Dangl, J. L. & Jones, J. D. Plant pathogens and integrated defence responses to infection. *Nature* **411**, 826–833 (2001).
12. Dodds, P. N. & Rathjen, J. P. Plant immunity: towards an integrated view of plant–pathogen interactions. *Nat. Rev. Genet.* **11**, 539–548 (2010).
13. Oliva, R. et al. Broad-spectrum resistance to bacterial blight in rice using genome editing. *Nat. Biotechnol.* **37**, 1344–1350 (2019).
14. Lapin, D. & Van den Ackerveken, G. Susceptibility to plant disease: more than a failure of host immunity. *Trends Plant Sci.* **18**, 546–554 (2013).
15. Vogel, J. P., Raab, T. K., Schiff, C. & Somerville, S. C. *PMR6*, a pectate lyase–like gene required for powdery mildew susceptibility in Arabidopsis. *Plant Cell* **14**, 2095–2106 (2002).
16. Eckardt, N. A. Plant disease susceptibility genes? *Plant Cell* **14**, 1983–1986 (2002).
17. Kim, M. C. et al. Calmodulin interacts with MLO protein to regulate defence against mildew in barley. *Nature* **416**, 447–451 (2002).
18. Devoto, A. et al. Topology, subcellular localization, and sequence diversity of the Mlo family in plants. *J. Biol. Chem.* **274**, 34993–35004 (1999).
19. Kusch, S. & Panstruga, R. *mlo*-based resistance: an apparently universal "weapon" to defeat powdery mildew disease. *Mol. Plant Microbe Interact.* **30**, 179–189 (2017).
20. Wang, Y. et al. Simultaneous editing of three homoeoalleles in hexaploid bread wheat confers heritable resistance to powdery mildew. *Nat. Biotechnol.* **32**, 947–951 (2014).
21. Bai, Y. et al. Naturally occurring broad-spectrum powdery mildew resistance in a Central American tomato accession is caused by loss of *Mlo* function. *Mol. Plant Microbe Interact.* **21**, 30–39 (2008).
22. Humphry, M., Consonni, C. & Panstruga, R. *mlo*-based powdery mildew immunity: silver bullet or simply non-host resistance? *Mol. Plant Pathol.* **7**, 605–610 (2006).
23. Piffanelli, P. et al. A barley cultivation-associated polymorphism conveys resistance to powdery mildew. *Nature* **430**, 887–891 (2004).
24. Acevedo-Garcia, J., Kusch, S. & Panstruga, R. Magical mystery tour: MLO proteins in plant immunity and beyond. *New Phytol.* **204**, 273–281 (2014).
25. Appiano, M. et al. Monocot and dicot MLO powdery mildew susceptibility factors are functionally conserved in spite of the evolution of class-specific molecular features. *BMC Plant Biol.* **15**, 257 (2015).
26. Singh, R. P. et al. Disease impact on wheat yield potential and prospects of genetic control. *Annu. Rev. Phytopathol.* **54**, 303–322 (2016).
27. Acevedo-Garcia, J. et al. *mlo*-based powdery mildew resistance in hexaploid bread wheat generated by a non-transgenic TILLING approach. *Plant Biotechnol. J.* **15**, 367–378 (2017).
28. Bogdanove, A. J. & Voytas, D. F. TAL effectors: customizable proteins for DNA targeting. *Science* **333**, 1843–1846 (2011).
29. Ramírez-González, R. H. et al. The transcriptional landscape of polyploid wheat. *Science* **361**, eaar6089 (2018).
30. Wormit, A. et al. Molecular identification and physiological characterization of a novel monosaccharide transporter from *Arabidopsis* involved in vacuolar sugar transport. *Plant Cell* **18**, 3476–3490 (2006).
31. Bieluszewski, T., Xiao, J., Yang, Y. & Wagner, D. PRC2 activity, recruitment, and silencing: a comparative perspective. *Trends Plant Sci.* **21**, S1360–S1385 (2021).
32. Kajimura, T., Mizuno, N. & Takumi, S. Utility of leaf senescence-associated gene homologs as developmental markers in common wheat. *Plant Physiol. Biochem.* **48**, 851–859 (2010).
33. Consonni, C. et al. Tryptophan-derived metabolites are required for antifungal defense in the *Arabidopsis mlo2* mutant. *Plant Physiol.* **152**, 1544–1561 (2010).
34. Gao, C. Genome engineering for crop improvement and future agriculture. *Cell* **184**, 1621–1635 (2021).
35. Zhang, Y. et al. Efficient and transgene-free genome editing in wheat through transient expression of CRISPR/Cas9 DNA or RNA. *Nat. Commun.***7**, 12617–12624 (2016).
36. Liang, Z. et al. Efficient DNA-free genome editing of bread wheat using CRISPR/Cas9 ribonucleoprotein complexes. *Nat. Commun.***8**, 14261–14265 (2017).
37. Jansen, M., Jarosch, B. & Schaffrath, U. The barley mutant *emr1* exhibits restored resistance against *Magnaporthe oryzae* in the hypersusceptible *mlo*-genetic background. *Planta* **225**, 1381–1391 (2007).

Publisher's note Springer Nature remains neutral with regard to jurisdictional claims in published maps and institutional affiliations.

© The Author(s), under exclusive licence to Springer Nature Limited 2022

Methods

Plant materials and growth conditions

Wheat (*T. aestivum*) used in this study was Bobwhite (spring wheat) unless otherwise stated, including Kenong199 (KN199, winter wheat), *Tamlo-aabbdd* (KN199) (*TaMLO1* knockout mutant in a KN199 background[20]). *A. thaliana* wild type (Col-0) and the mutant *Atmlo2/6/12* (ref. [4]) were also used.

Wheat was grown in a growth room under a 16 h light:8 h dark cycle with light intensity 1,000 μmol m^{-2} s^{-1}, and temperature 15–26 °C depending on growth stage; *Arabidopsis* was grown under an 8 h light:16 h dark cycle (short-day conditions) or a 16 h light:8 h dark cycle (long-day conditions), with light intensity 100 μmol m^{-2} s^{-1}, at a constant 23 °C. Wheat was also grown in the field in two wheat-growing areas in the North China Plain: Beijing and Zhaoxian in Hebei Province. Spring wheat varieties were sown in March, and winter wheat varieties in October, and harvested the following June. Field trials were performed with three replicates at each site. Each replicate used a plot 0.75 m (4 rows) in width (0.25 m row spacing) by 3 m in length (0.1 m plant spacing). Agronomical traits were recorded from ~30 individuals in the central rows of each plot. Field trials were conducted in two cropping years, 2019 and 2020. Statistical significance was determined by two-tailed Mann–Whitney tests or two-tailed Student's *t*-tests, using GraphPad Software. *P* values > 0.05 were considered not significant.

Constructs for gene overexpression and genome editing

To overexpress *TaTMT3B* in wheat, the full-length coding region was amplified from cDNA, and cloned into pJIT163-Ubi vector[20]. To overexpress *AtTMT3* in *Arabidopsis*, the full-length coding sequence was cloned into pCambia1300-35S vector[38]. For wheat genome editing, plasmid constructs pJIT163-Ubi-Cas9 (ref. [20]) and pU6-gRNA[39] were used, as previously described. Sequences of PCR primers and other oligonucleotides used for construction are listed in Supplemental Table 1.

Genetic transformation of wheat and *Arabidopsis*

Plasmids DNA vectors and RNPs (synthesized sgRNAs and Cas9 protein were purchased from GenScript Nanjing) were delivered into immature wheat embryos via particle bombardment. In order to avoid mixing up RNP-generated mutants with those derived from plasmid transformation, we used another sgRNA, sgRNA2-2 (with comparable indel efficiency to sgRNA2-1) to target *TaMLOX*. The subsequent callus induction, plantlet regeneration and selection were performed as previously described[39,40]. T_0 transgenic plants were obtained, transferred to soil and grown in a growth room. Floral-dipping transformation of *Arabidopsis* was carried out following the standard protocol[41].

Powdery mildew infection assays

B. graminis f. sp. *tritici* (*Bgt*) isolate E09 (ref. [42]) and isolate GH5 (a local virulent *Bgt* isolate for LX99 and JM22, obtained from plant material spontaneously infected in the greenhouse) was propagated on wheat KN199 seedlings in a growth chamber with a 16 h photoperiod, 60% humidity, at a constant 22 °C. *Golovinomyces orontii*[43] was propagated on *Arabidopsis NahG* plants in a growth chamber with an 8 h photoperiod, 60% humidity, at a constant 22 °C. Powdery mildew inoculation and microscopic analyses were performed as previously reported[4,20]. Seventy-two hours after inoculation, wheat leaf segments and *Arabidopsis* leaves were harvested and de-stained, then stored in lactoglycerol (1:1:1(v/v/v) lactic acid/glycerol/water). Fungal structures were stained for 7 s with 0.6% (w/v) Coomassie Brilliant Blue R 250 in methanol, then rinsed with distilled water and mounted in 50% (v/v) glycerol. Samples were observed and counted under an Olympus BX51 light microscope, and photographs were taken with Cellsens Entry 1.21 software. Percentages of microcolonies formed from the total number of *B. graminis* or *G. orontii* germinated spores on the leaves of the indicated plants. More than 600 germinated spores were examined per genotype per experiment. For macroscopic infection phenotype, detached leaves of 7-day post-inoculation plants were photographed.

Genotyping by PCR and whole-genome sequencing

To identify mutations in *TaMLO-A1*, *TaMLO-B1*, or *TaMLO-D1*, gene-specific primers were designed around the target site. Primers F1 and R1 were used to amplify *TaMLO-A1*, F2 and R2 were used to amplify *TaMLO-B1*, and F3 and R3 were used to amplify *TaMLO-D1*. To determine the precise location of the rearrangement breakpoints in the B genome of the *Tamlo-R32* mutant, primers F4 and R4 were used to amplify the regions around the deletion. PCR products were checked on agarose gels and genotyped by Sanger sequencing. Primers are listed in Supplementary Table 1.

For whole-genome sequencing by NGS, high-quality genomic DNA was isolated using a GenElute Plant Genomic DNA Miniprep Kit (Sigma-Aldrich). Illumina NGS libraries were prepared according to the manufacturer's protocols, and sequencing was performed on a Novaseq PE150 platform. An average of 800 Gb of data (~50-fold coverage) was generated. Sequencing reads were mapped to the China Spring wheat reference genome (IWGSC, Refseq v1.1), and assigned to a specific location within an estimated 0.7 Mb window around *TaMLO-B1*. Sam files generated from BWA[44] were converted to bam files and further sorted and indexed with samtools (1.9)[45]. To visualize the large deletion shown in Fig. 1g, an Integrative Genomics Viewer (2.8.13)[46] was used with bam file input.

RNA isolation and quantitative RT–PCR

Total RNA was isolated using Trizol reagent (Invitrogen). After removing genomic DNA with DNase, total RNA was reverse-transcribed into complementary DNAs (cDNAs) with oligo(dT)20 using a Superscript IV First-Strand Synthesis System (Thermo Fisher Scientific). To quantify the relative abundance of transcripts, quantitative PCR was carried out using a SYBRGreen Realtime PCR Master Mix (TaKaRa) on a CFX real-time PCR amplifier (Bio-Rad). Three independent RNA preparations were used as biological replicates. *TaACTIN* (TraesCS5B02G124100) and *TaPARG* (TraesCS5B02G532300) (a housekeeping gene selected from RNA-seq data based on its ubiquitous expression in all tissues[29]) were used as internal control for normalization in wheat and *AtACTIN8* (AT1G49240) in *Arabidopsis*, respectively. Gene expression levels were determined by the $2^{-\Delta\Delta Ct}$ method, unless otherwise stated. The primers used are listed in Supplementary Table 1.

RNA-seq and data processing

Leaves from 7-day-old wheat plants grown in a controlled condition were collected, immediately snap-frozen and stored at −80 °C. Total RNA was extracted using a RiboPure kit (Invitrogen). RNA-seq experiments were performed with three independent biological replicates. An RNA-seq library was constructed and sequenced using the Illumina NovaSeq platform by Annoroad Gene Technology. Raw reads were filtered with fastp (version 0.20.1) and aligned to the Chinese Spring genome (IWGSC RefSeq v1.1) using hisat2 (version 2.1.0)[47]. Raw counts per gene were quantified using FeatureCount (version 1.6.4)[48]. An R package edgeR[49] was used to detect DEGs (differentially expressed genes), with a threshold absolute value of $\log_2$(fold change) ≥ 1 and FDR ≤ 0.05. The raw matrix was further normalized to transcripts per kilobase million (TPM) to quantify gene expression.

Chromosome conformation capture assays

4C was used to discover potential chromatin loops linked to *TaTMT3B* promoter. 4C libraries were constructed following previously described protocols with some modifications[50,51]. NcoI and DpnII were used as the primary and secondary restriction enzymes, respectively. The nuclei isolation followed the HiChIP method[52] and the first restriction enzyme digestion and ligation reactions were performed as described by In-situ HiC[53]. The 4C library was sequenced using Illumina NovaSeq platform with paired ends (PE150) at Annoroad Gene Technology.

The purified DNA from first-round digestion and ligation was used for 3C–qPCR to validate and quantify the chromatin loops discovered via 4C-seq. For a–c loop, we used 6 bp-cutter digestion (NcoI), while for relative shorter-range a–b loop, 4 bp-cutter digestion (DpnII) was used to achieve better resolution. qPCR was performed using the TaqMan probe method according to the manufacturer's instructions, with an AceQ qPCR Probe Master Mix (Vazyme Biotech). Relative interaction frequencies were calculated according to previous publication[54]. We used ADP ribosylation factor (ADP-RF) coding gene as loading control to normalize the variations in DNA concentration between 3C samples[55].

ATAC-seq and data processing

ATAC-seq was performed according to previous publication with minor modifications[56]. Approximately 1 g of leaves was used for starting material. About 50,000 clean and intact nuclei were used for tagmentation per reaction. Libraries were purified with AMPure beads (Beckman, A63881) and sequenced using the Illumina Novaseq platform with paired ends (PE150) at Annoroad Gene Technology. Peaks of ATAC-seq were identified using MACS2[57]. Coverage tracks were generated from aligned reads using DeepTools with RPKM normalization (version 3.5.0)[58]. The tracks were displayed using an Integrative Genomics Viewer[46].

CUT&Tag assay for histone modification and data processing

The CUT&Tag assay was performed as reported[59], with minor modifications. Nuclei were extracted following the ATAC-seq procedure as described above. For each reaction, about 10,000 nuclei were used. Histone antibodies including H3K27ac (Abcam, ab4729), H3K27me3 (Abcam, ab6002), H3K4me3 (Abcam, ab8580), and H3K36me3 (Abcam, ab9050) were used as primary antibodies at 1:50 dilutions. Guinea pig anti-rabbit IgG was used as secondary antibody at 1:100 dilutions. The library was amplified by about 15 cycles using Q5 high fidelity polymerase (NEB), and purified with AMPure XP beads (Beckman, A63881) and sequenced with Novaseq PE 150. All sequencing reads were cleaned with fastp (version 0.20.1)[60] and mapped to the Chinese Spring genome using the BWA mem algorithm (version 0.7.15-r1140)[44]. To obtain high quality data, the mapped reads were filtered for MAPQ quality scores above 30, and uniquely aligned with Samtools (version 1.9). Picard (http://broadinstitute.github.io/picard/) was used to remove duplicates. Peaks were called by MACS2[57].

ChIP followed by quantitative PCR for Pol II profiling

ChIP was performed as previously described[61], with minor modifications. Extraction buffers I (0.4 M sucrose, 10 mM Tris-HCl, pH 8.0, 10 mM $MgCl_2$, 5 mM β-mercaptoethanol, 1 mM PMSF, 1× protease inhibitor (Roche)) and II (0.25 M sucrose, 10 mM Tris-HCl, pH 8.0, 10 mM $MgCl_2$, 1% Triton X-100, 5 mM β-mercaptoethanol, 1 mM PMSF, 1× protease inhibitor (Roche)) were used for protein extraction. Anti-Pol II CTD-S5p (Abcam, ab5408) antibody was used for ChIP. Pol II abundance was normalized over input.

Chlorophyll content

For wheat, we measured relative chlorophyll content with a hand-held chlorophyll meter (SPAD-502; Minolta). SPAD values indicated relative amounts of total chlorophyll in plant leaves[62]. Measurements were performed on 3rd leaves (distal to the flag leaf) to the flag leaf at the heading stage. Four measurements were made per leaf from at least six individual plants of each genotype. For *Arabidopsis*, chlorophyll content was determined as described, with minor modifications[63,64]. In brief, chlorophyll was isolated from leaves by homogenization in liquid nitrogen and extraction in 80% (v/v) acetone. After centrifugation (2 min, 16,000*g*), the supernatant was used to measure absorbance values at 663 nm and 645 nm by a spectrophotometer, with 80% acetone as control. Three biological replicates of each sample were assayed.

Developing new wheat germplasms harboring the *Tamlo-R32* mutation by marker-assisted selection

Liangxing99 (LX99) and Jimai22 (JM22), major elite cultivars in the Northern Huang-Huai River Valley Winter Wheat Region of China, were selected to cross with *Tamlo-R32* to develop new wheat germplasms though MAS. The hybrids were backcrossed with LX99 and JM22 for two generations. BC_2F_1 plants with mutations in the A, B and D genomes were selected using the four markers F1/R1, F2/R2, F3/R3, and F4/R4 flanking *TaMLO1* or the large deletion, and then self-fertilized. BC_2F_2 plants carrying recessive homozygous alleles for *TaMLO-A1*, *TaMLO-D1*, and the large deletion in the B genome were selected by MAS and evaluated for powdery mildew resistance by infecting detached leaves. In order to evaluate the effects of the new *Tamlo-R32* allele on the recipient cultivars, the heights and grain yields per plant of BC_2F_3 homozygous plants were measured in the greenhouse.

Statistical analysis

Normal distributions were tested with the Shapiro–Wilk normality test. Sample size *n* means number of biological replicates, unless specifically stated. GraphPad Prism 8.0.1 (GraphPad Software) was used for all statistical analyses. Statistical significance was determined by two-tailed Mann–Whitney tests or two-tailed Student's *t*-tests. *P* values > 0.05 were considered non-significant. Sample sizes, statistical tests used and *P* values are stated in the figures or figure legends.

Reporting summary

Further information on research design is available in the Nature Research Reporting Summary linked to this paper.

Data availability

The sequencing data obtained in this study have been deposited in the Genome Sequence Archive (GSA) database in the BIG Data Center (https://ngdc.cncb.ac.cn/) under accession number PRJCA005687. Chinese Spring wheat reference genome RefSeq v1.1 is available on IWGSC (http://www.wheatgenome.org/). Transcriptome data from different wheat tissues are from ref. [29]. Source data are provided with this paper.

38. Li, S. et al. MYB75 phosphorylation by MPK4 is required for light-induced anthocyanin accumulation in *Arabidopsis*. *Plant Cell* **28**, 2866–2883 (2016).
39. Shan, Q. et al. Targeted genome modification of crop plants using a CRISPR–Cas system. *Nat. Biotechnol.* **31**, 686–688 (2013).
40. Liang, Z. et al. Genome editing of bread wheat using biolistic delivery of CRISPR/Cas9 in vitro transcripts or ribonucleoproteins. *Nat. Protoc.* **13**, 413–430 (2018).
41. Clough, S. J. & Bent, A. F. Floral dip: a simplified method for *Agrobacterium*-mediated transformation of *Arabidopsis thaliana*. *Plant J.* **16**, 735–743 (1998).
42. Wang, Z. et al. Genetic and physical mapping of powdery mildew resistance gene *MlHLT* in Chinese wheat landrace Hulutou. *Theor. Appl. Genet.* **128**, 365–373 (2015).
43. Shen, Q. H. et al. Nuclear activity of MLA immune receptors links isolate-specific and basal disease-resistance responses. *Science* **315**, 1098–1103 (2007).
44. Li, H. & Durbin, R. Fast and accurate short read alignment with Burrows–Wheeler transform. *Bioinformatics* **25**, 1754–1760 (2009).
45. Danecek, P. et al. Twelve years of SAMtools and BCFtools. *Gigascience* **10**, giab008 (2021).
46. Thorvaldsdóttir, H., Robinson, J. T. & Mesirov, J. P. Integrative Genomics Viewer (IGV): high-performance genomics data visualization and exploration. *Brief Bioinform.* **14**, 178–192 (2013).
47. Kim, D., Paggi, J. M., Park, C., Bennett, C. & Salzberg, S. L. Graph-based genome alignment and genotyping with HISAT2 and HISAT-genotype. *Nat. Biotechnol.* **37**, 907–915 (2019).
48. Liao, Y., Smyth, G. K. & Shi, W. featureCounts: an efficient general purpose program for assigning sequence reads to genomic features. *Bioinformatics* **30**, 923–930 (2014).
49. Robinson, M. D., McCarthy, D. J. & Smyth, G. K. edgeR: a Bioconductor package for differential expression analysis of digital gene expression data. *Bioinformatics* **26**, 139–140 (2010).
50. Weber, B., Jamge, S. & Stam, M. 3C in maize and *Arabidopsis*. *Methods Mol. Biol.* **1675**, 247–270 (2018).
51. Krijger, P. H., Geeven, G., Bianchi, V., Hilvering, C. R., & de Laat, W. 4C-seq from beginning to end: a detailed protocol for sample preparation and data analysis. *Methods* **170**, 17–32. (2020).
52. Ricci, W. A. et al. Widespread long-range *cis*-regulatory elements in the maize genome. *Nat. Plants* **5**, 1237–1249 (2019).

53. Rao, S. S. et al. A 3D map of the human genome at kilobase resolution reveals principles of chromatin looping. *Cell* **159**, 1665–1680 (2014).
54. Kim, D. & Sung, S. Vernalization-triggered intragenic chromatin-loop formation by long noncoding RNAs. *Dev. Cell* **40**, 302–312 (2017).
55. Paolacci, A. R., Tanzarella, O. A., Porceddu, E. & Ciaffi, M. Identification and validation of reference genes for quantitative RT–PCR normalization in wheat. *BMC Mol. Biol.* **10**, 11 (2009).
56. Bajic, M., Maher, K. A. & Deal, R. B. Identification of open chromatin regions in plant genomes using ATAC-seq. *Methods Mol. Biol.* **1675**, 183–201 (2018).
57. Zhang, Y. et al. Model-based analysis of ChIP-seq (MACS). *Genome Biol.* **9**, R137 (2008).
58. Ramírez, F., Dündar, F., Diehl, S., Grüning, B. A. & Manke, T. deepTools: a flexible platform for exploring deep-sequencing data. *Nucleic Acids Res.* **42**, W187–W191 (2014).
59. Kaya-Okur, H. S. et al. CUT&Tag for efficient epigenomic profiling of small samples and single cells. *Nat. Commun.* **10**, 1930 (2019).
60. Chen, S., Zhou, Y., Chen, Y. & Gu, J. fastp: an ultra-fast all-in-one FASTQ preprocessor. *Bioinformatics* **34**, i884–i890 (2018).
61. Xiao, J. et al. *Cis*- and *trans*-determinants of epigenetic silencing by Polycomb Repressive Complex 2 in *Arabidopsis*. *Nat. Genet.* **49**, 1546–1552 (2017).
62. Gou, J. Y. et al. Wheat stripe rust resistance protein WKS1 reduces the ability of the thylakoid-associated ascorbate peroxidase to detoxify reactive oxygen species. *Plant Cell* **27**, 1755–1770 (2015).
63. Qin, D. et al. Characterization and fine mapping of a novel barley *Stage Green-Revertible Albino* gene (*HvSGRA*) by bulked segregant analysis based on ssr assay and specific length amplified fragment sequencing. *BMC Genomics* **16**, 838–851 (2015).
64. Ni, Z. et al. Altered circadian rhythms regulate growth vigour in hybrids and allopolyploids. *Nature* **457**, 327–331 (2009).

Acknowledgements This work was supported by grants from the Strategic Priority Research Program of the Chinese Academy of Sciences (XDA24020101 to J.-L.Q., XDA24020102 to C.G., XDA24010204 to J.X., XDA24020310 to Y.W., XDPB16 to J.-L.Q.), the National Natural Science Foundation of China (31788103 to C.G., 32001891 to S.L., 31970529 to J.X. and 31971370 to K.C.) and the Key Research Program of Frontier Sciences (QYZDY-SSW-SMC030 to C.G.) and the Youth Innovation Promotion Association of the Chinese Academy of Sciences (2020000003 to Y.W.).

Author contributions C.G. and J.-L.Q. conceived and conceptualized the study. C.G. and J.-L.Q. designed the experiments. S.L., D.L. and Y.Z. performed most of the experiments. S.L., Y.W. and J.X. prepared the figures. S.L. and Y.Z. performed the powdery mildew infection experiment. D.L., B. Li, Y. Lei, J.L. and K.C carried out genome-editing experiments and mutant identification. M.D. conducted the 4C and 3C experiments. L.Z. and J.X. conducted the CUT&Tag, ATAC-seq and bioinformatics analyses. B. Lv, and Y. Liang performed the marker-assisted selection (MAS) and powdery mildew microscopic analyses. S.L. and Y.W. characterized the phenotypes of mutant plants. Y.C. and Z.L. carried out traditional breeding and field trials. J.-L.Q., C.G., S.L. and J.X wrote the manuscript. All authors commented on the results and contributed to the manuscript.

Competing interests C.G., J.-L.Q., S.L. and Y.W. have filed patent applications based on the work published here.

Additional information

Supplementary information The online version contains supplementary material available at https://doi.org/10.1038/s41586-022-04395-9.

Correspondence and requests for materials should be addressed to Jun Xiao, Jin-Long Qiu or Caixia Gao.

Peer review information *Nature* thanks Wendy Harwood, Nian Wang and the other, anonymous, reviewers for their contribution to the peer review of this work. Peer review reports are available.

Reprints and permissions information is available at http://www.nature.com/reprints.

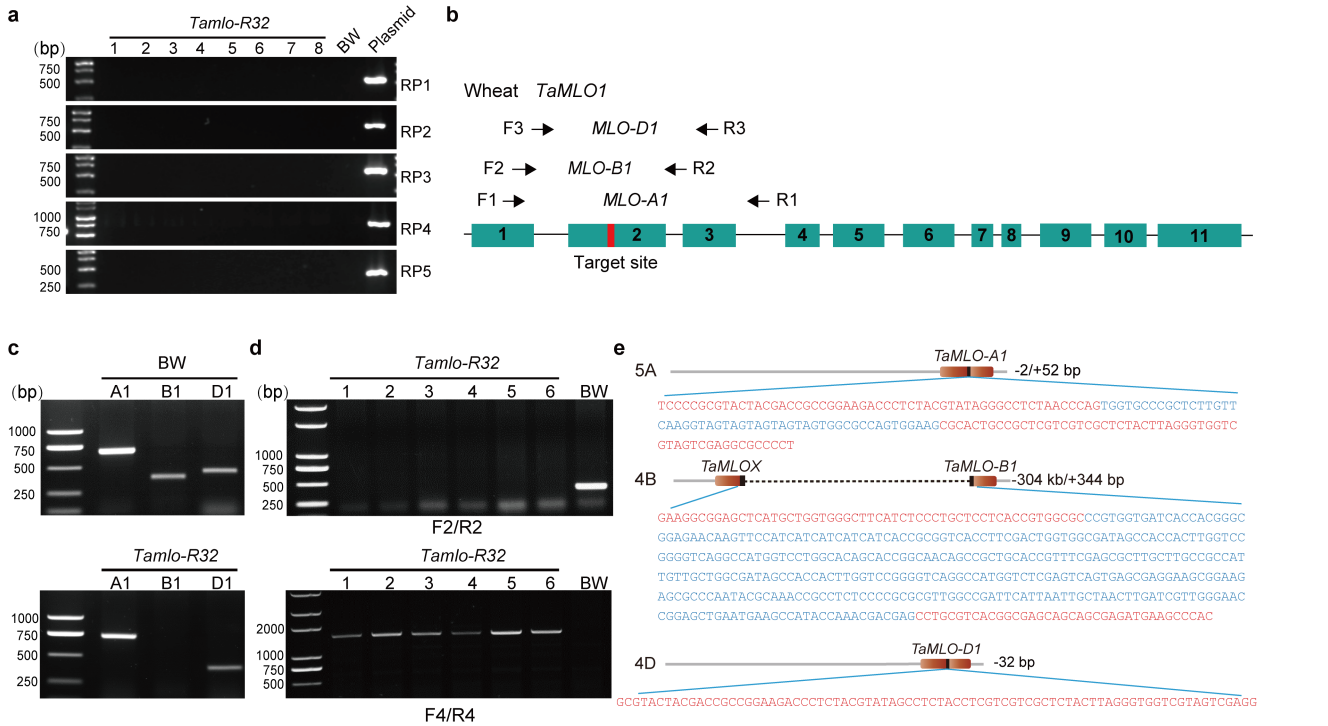

Extended Data Fig. 1 | Genotyping by agarose gel electrophoresis and Sanger sequencing. a, Detection of the transgene in the *Tamlo-R32* mutants by PCR using five independent primer sets. Plasmid DNA of the TALEN vector was used as a positive control. **b**, Schematic diagram of the structure of the wheat *TaMLO1* gene. Green rectangles and solid black lines represent exons and introns, respectively. The conserved TALEN target site within *TaMLO1* is indicated by the red vertical line. Black arrows denote the positions and orientations of the three pairs of gene-specific primers (F1/R1, F2/R2, F3/R3) for amplifying *TaMLO-A1, TaMLO-B1* and *TaMLO-D1*, respectively. **c**, Agarose gel electrophoresis of *TaMLO1* amplicons from genomic DNA of the BW wild-type (upper) and *Tamlo-R32* mutant (lower) using gene-specific primers. **d**, Agarose gel electrophoresis of the PCR products amplified by the primer pairs F2/R2 (upper) and F4/R4 (lower) from genomic DNA of the wild type and *Tamlo-R32* mutants. The positions and orientations of the F4/R4 primer pairs are denoted by black arrows in Fig. 1g. **e**, DNA sequence of the edited sites in *Tamlo-R32*. Blue letters indicate inserted sequences. Red letters indicate the original sequence. Black vertical lines indicate the target site. The black dotted line indicates the deleted region. For **a**, **c**, **d**, experiments were repeated 3 times with the same results.

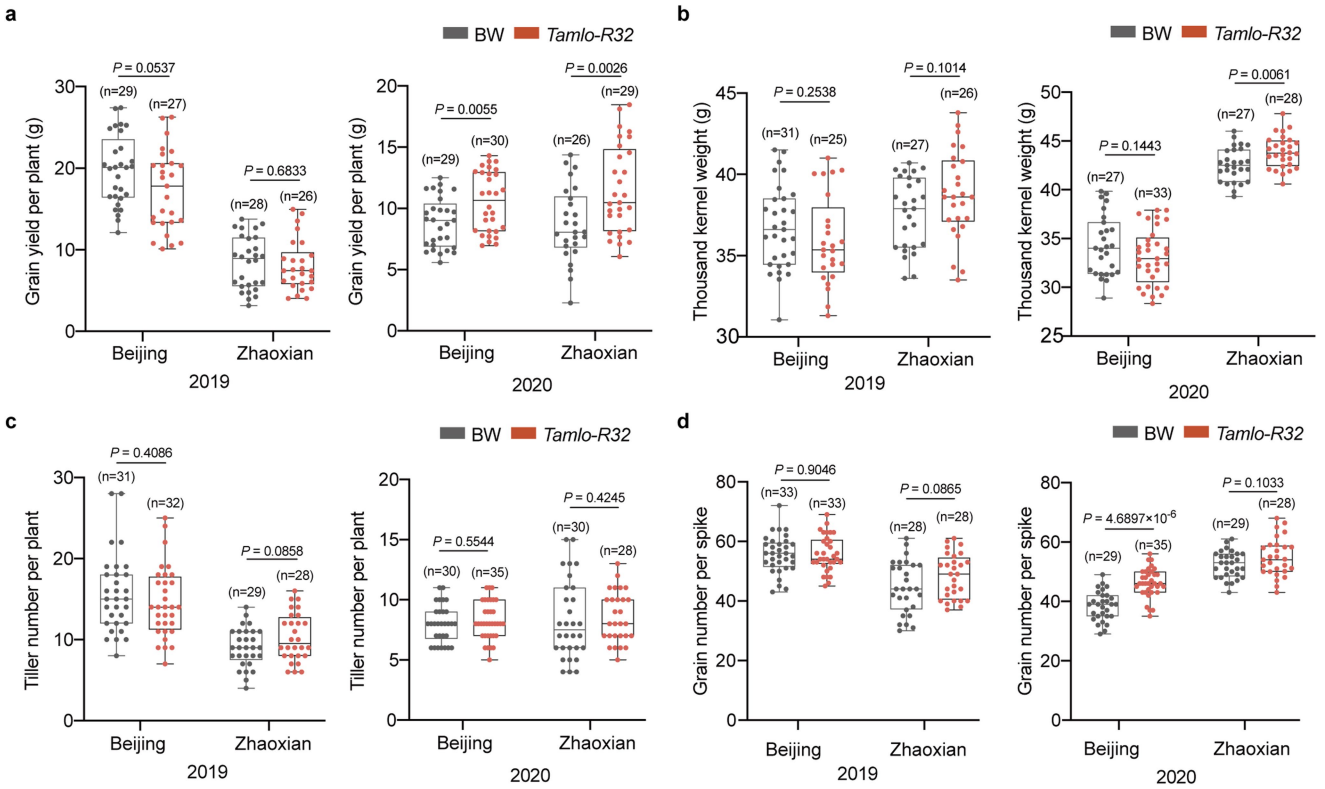

Extended Data Fig. 2 | The *Tamlo-R32* mutant displays no yield penalties when grown in the field. a–d, The agronomic traits, including grain yield per plant (**a**), thousand kernel weight (**b**), tiller number per plant (**c**) and grain number per spike (**d**) were evaluated in field conditions in two wheat-growing areas in the North China Plain, Beijing and Zhaoxian in Hebei Province in 2019 and 2020. For box plots, the box limits indicate the twenty-fifth and seventy-fifth percentiles, the whiskers indicate the full range of the data, and the center line indicates the median. Individual data points are plotted. *n* represents the sample size. Statistical significance was determined by two-tailed Mann-Whitney tests or two-tailed Student's *t*-tests. *P* values are indicated.

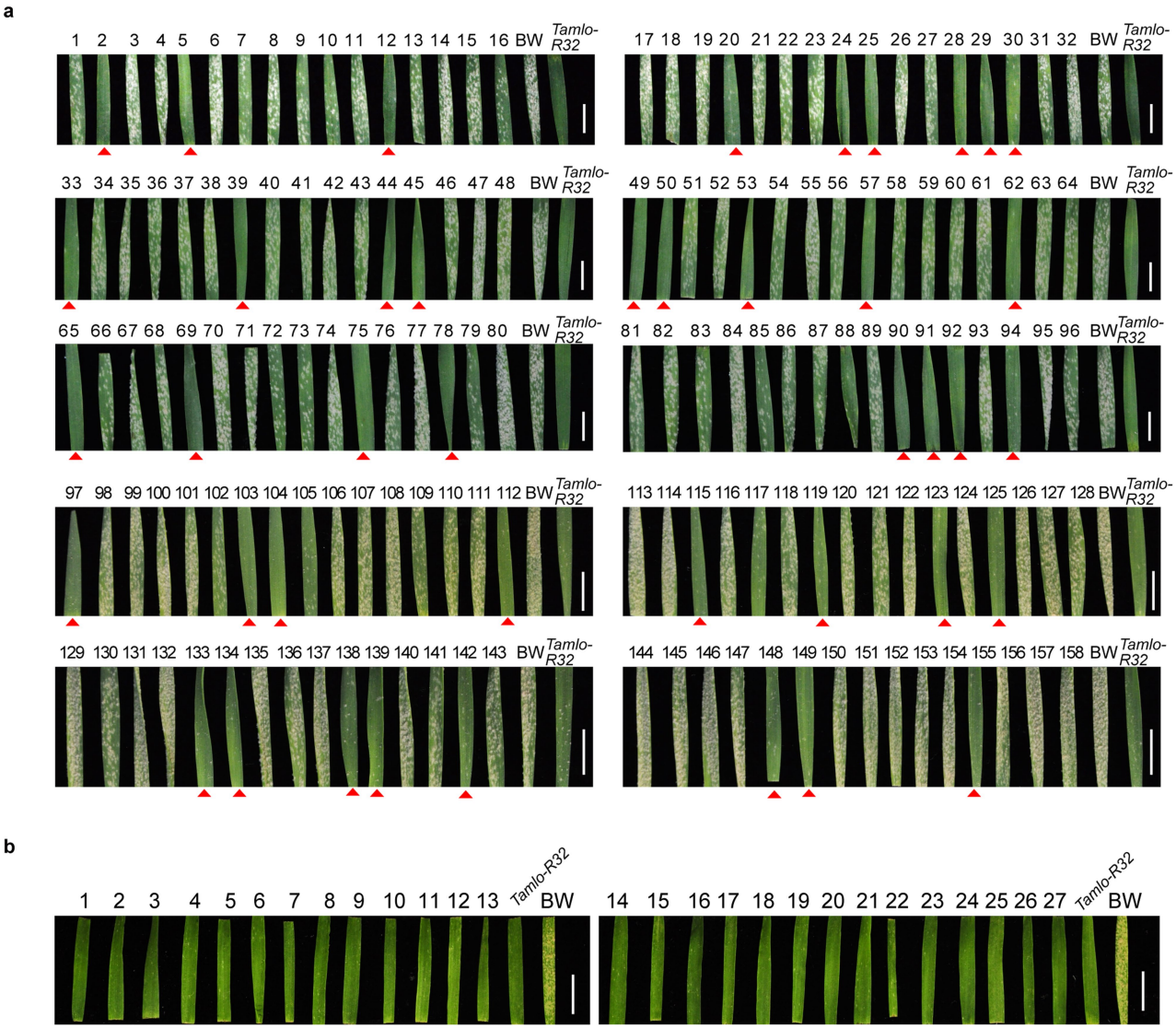

Extended Data Fig. 3 | Macroscopic powdery mildew infection phenotypes of F_2 plants from various crosses. a, b, Representative detached leaves of the F_2 generations of *Tamlo-R32*×*Tamlo-aaBBdd* (**a**) and *Tamlo-R32*×*Tamlo-aabbdd* (**b**) are shown seven days after inoculation of *Bgt* isolate E09. Red triangles indicate resistant plants. Scale bar, 1 cm.

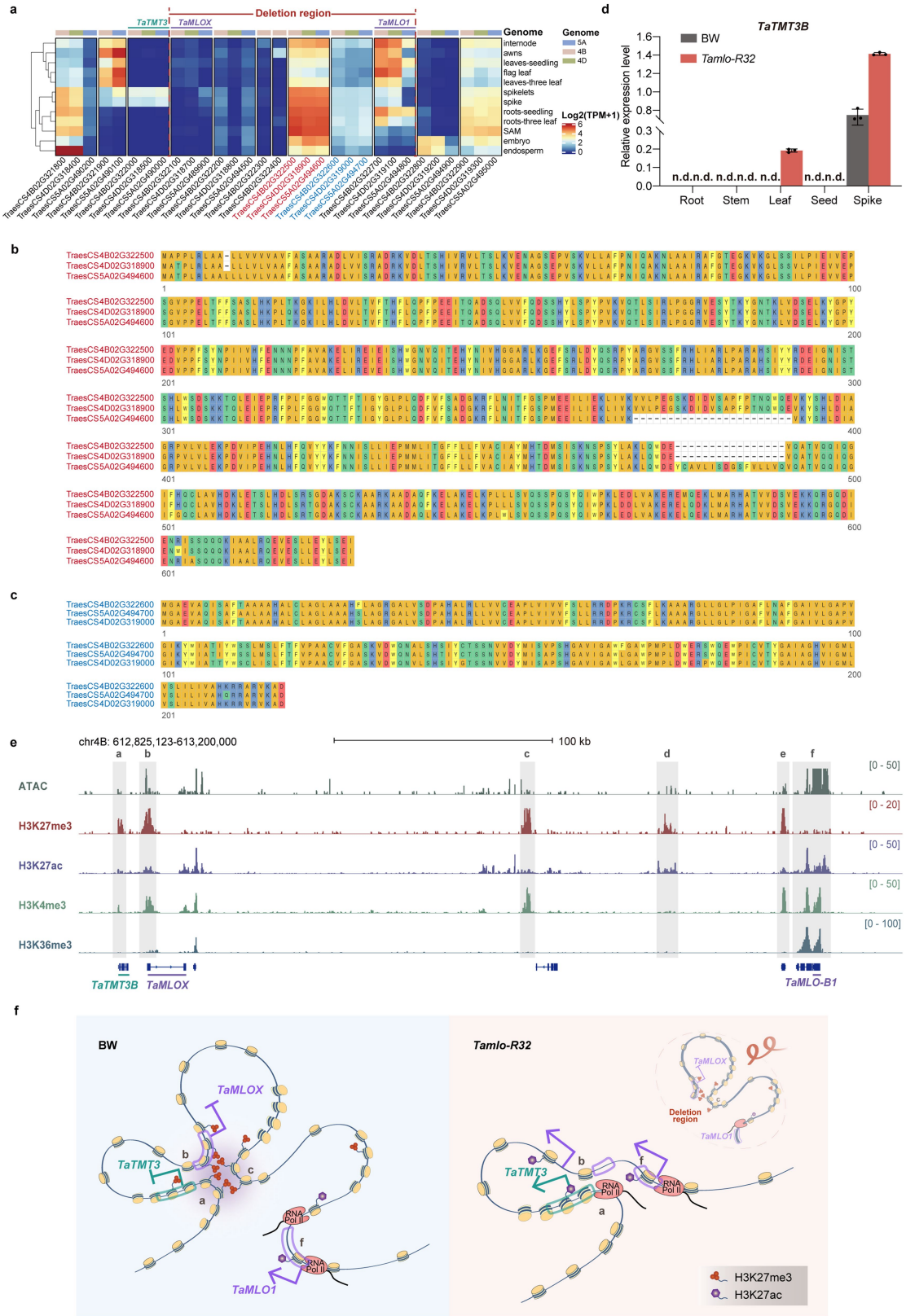

Extended Data Fig. 4 | See next page for caption.

Extended Data Fig. 4 | Expression patterns and chromatin landscapes of genes around the large deletion. a, Expression of *TaTMT3B* and 11 other nearby genes in different tissues; data are from a previous publication[30]. Genes within the deleted region are indicated. **b, c**, Amino acid sequence alignment between homeologs on the A, B and D genomes of downregulated genes in the deletion region. **d**, Expression levels of *TaTMT3B* in different tissues of *Tamlo-R32* and WT plants measured by quantitative RT-PCR. Results are normalized to *TaPAGE* gene. n.d., not detected. Data are means ± s.d., of three independent RNA preparations from biological replicates. **e**, Chromatin accessibility, and histone modification profiles in the *TaTMT3B-MLO-B1* region in leaf tissue of Chinese Spring wheat. The Integrative Genomics Viewer (IGV) views show the various chromatin status profiles near *TaTMT3B*. The y-axis represents signal enrichment computed from reads at each position normalized to the total number of reads (RPKM). The dark shading indicates regions with either repressive (H3K27me3) or active (H3K4me3, H3K36me3, H3K27ac) histone modifications (a-f). **f**, Schematic illustration of a possible model for regulation of the activation of *TaTMT3B* expression in *Tamlo-R32*.

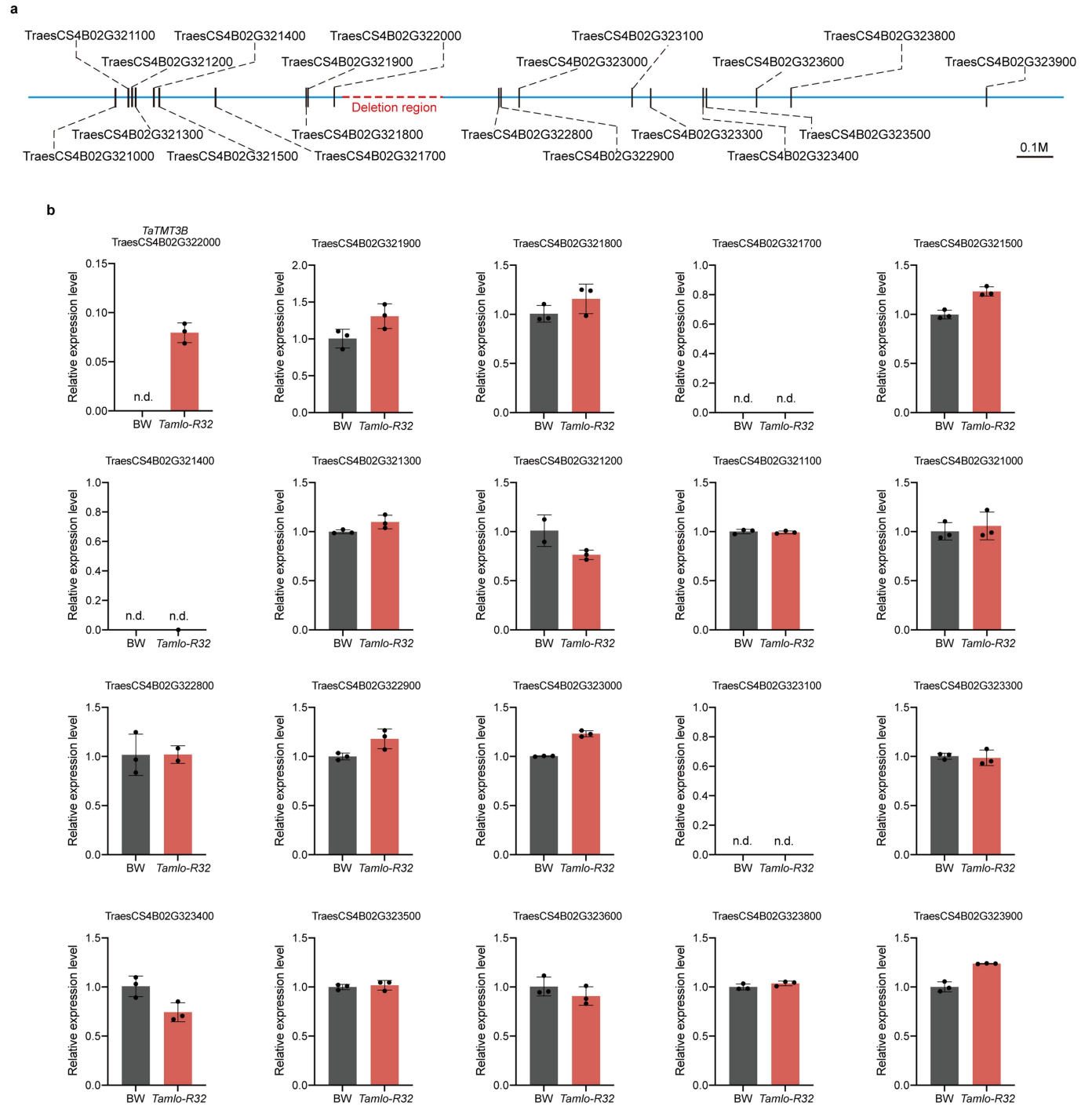

Extended Data Fig. 5 | Expression levels of twenty genes around the large deletion measured by quantitative RT-PCR. a, Schematic diagram of the gene distribution around the large B-genome deletion identified in *Tamlo-R32*. **b**, Expression levels of twenty genes of the B genome were measured by quantitative RT-PCR in both wild-type Bobwhite and *Tamlo-R32* mutant leaves. Results are normalized to *TaPARG* gene and the expression level of gene in wild-type BW plants was set at one except *TaTMT3B*. n.d., not detected. Data are means ± s.d. of three independent RNA preparations from biological replicates.

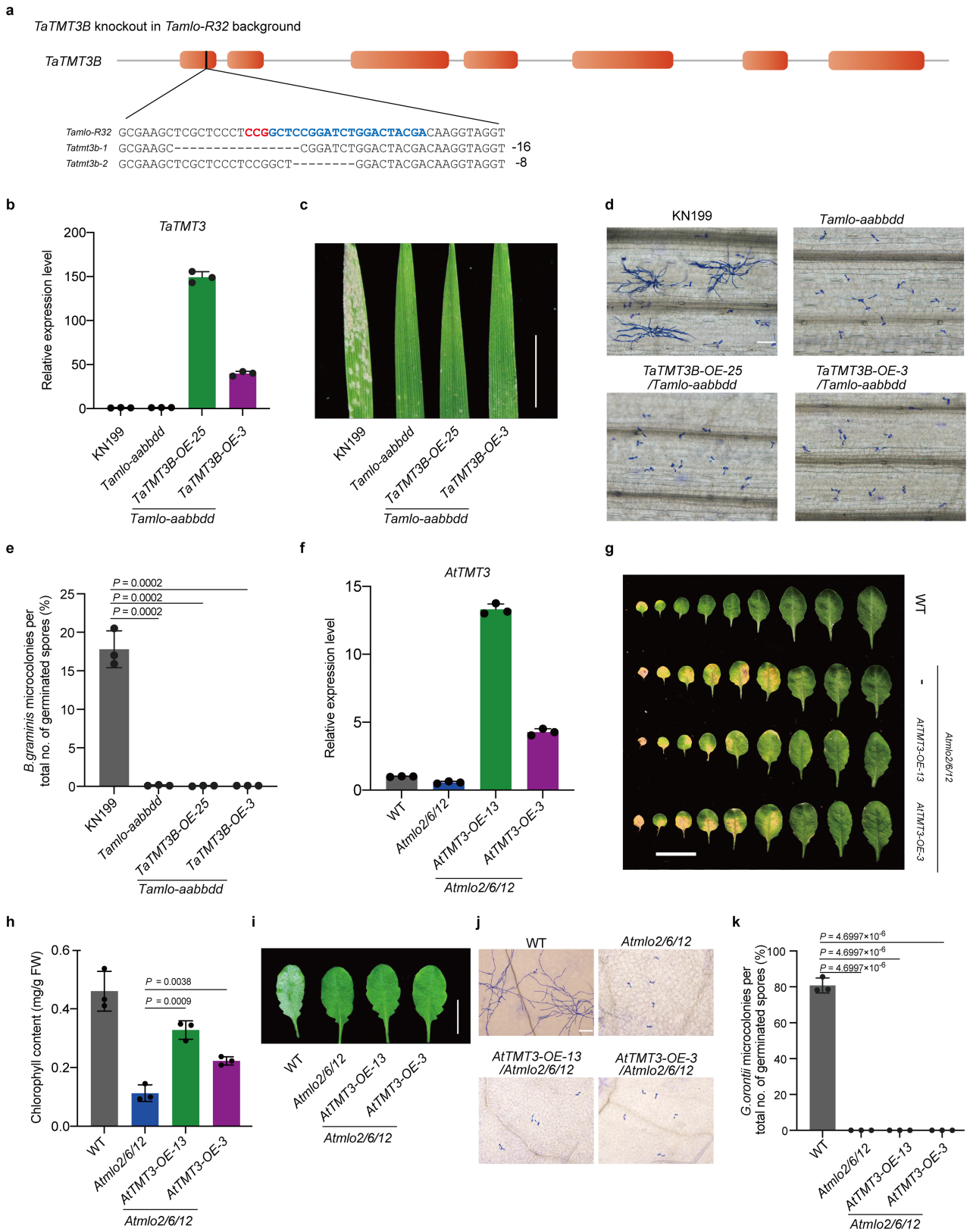

Extended Data Fig. 6 | See next page for caption.

Extended Data Fig. 6 | Wheat and *Arabidopsis mlo* mutants overexpressing *TMT3* maintain powdery mildew resistance. a, Targeted knockout of *TaTMT3B* by CRISPR-Cas9 in the *Tamlo-R32* background. Blue letters indicate *TaTMT3B* sgRNA. The PAM sequence is highlighted in red. The numbers on the right show the type of mutation and how many nucleotides are involved, with "-" indicating deletion of the given number of nucleotides. **b**, Expression levels of *TaTMT3* in *TaTMT3B*-overexpressors in the *Tamlo-aabbdd* mutant background, assessed by quantitative RT-PCR. The primers were designed to detect complete *TaTMT3* transcripts. The results are normalized to *TaACTIN*, and expression of the gene in KN199 (wild type) is set at one. Data are means ± s.d., of three independent RNA preparations from biological replicates. **c**, Macroscopic infection phenotypes of representative detached leaves of the indicated wheat plants seven days after inoculation with *Bgt* isolate E09. Scale bar, 1 cm. **d**, Micrographs of microcolony formation by *Bgt* on wheat leaves of the indicated genotypes three days postinoculation. Powdery mildew spores and colonies were stained with Coomassie blue. Scale bars, 100 µm. **e**, Percentages of microcolonies formed from the total number of germinated spores of *Bgt* on the leaves of the indicated wheat plants. **f**, Expression levels of *AtTMT3* in *TMT3*-overexpressors in the *Atmlo2/6/12* background measured by quantitative RT-PCR. The primers were designed to detect both transgenic and endogenous *AtTMT3* transcripts. The results are normalized to *Arabidopsis AtACTIN8*, and the expression level of the gene in WT was set at one. Data are means ± s.d. of three independent RNA preparations from biological replicates. **g**, Detached rosette leaves of the indicated 7-week-old *Arabidopsis* plants grown under long-day condition were laid out. Scale bar, 1 cm. **h**, Chlorophyll content of 6th rosette leaves of 7-week-old *Arabidopsis* plants grown under long-day conditions. The *Tamlo-aabbdd* mutants in **b**–**e** is in the KN199 background. Data are means of three biological replicates. Error bars represent means ± s.d. *P* values are indicated. **i**, Macroscopic infection phenotypes of representative detached leaves of the indicated *Arabidopsis* plants seven days after inoculation with *G. orontii* Scale bar, 1 cm. **j**, Micrographs of microcolony formation by *G. orontii* on *Arabidopsis* leaves of the indicated genotypes three days post-inoculation. Powdery mildew spores and colonies were stained with Coomassie blue. Scale bars, 100 µm. **k**, Percentages of microcolonies formed from the total number of germinated spores of *G. orontii* on leaves of indicated *Arabidopsis* plants. More than 1000 germinated spores per genotype per experiment were examined 72 h after inoculation in **e** and **k**. Data are means of three independent experiments. Error bars represent means ± s.d. Statistical significance in **e**, **h**, **k** was determined by two-tailed Mann-Whitney tests or two-tailed Student's *t*-tests.

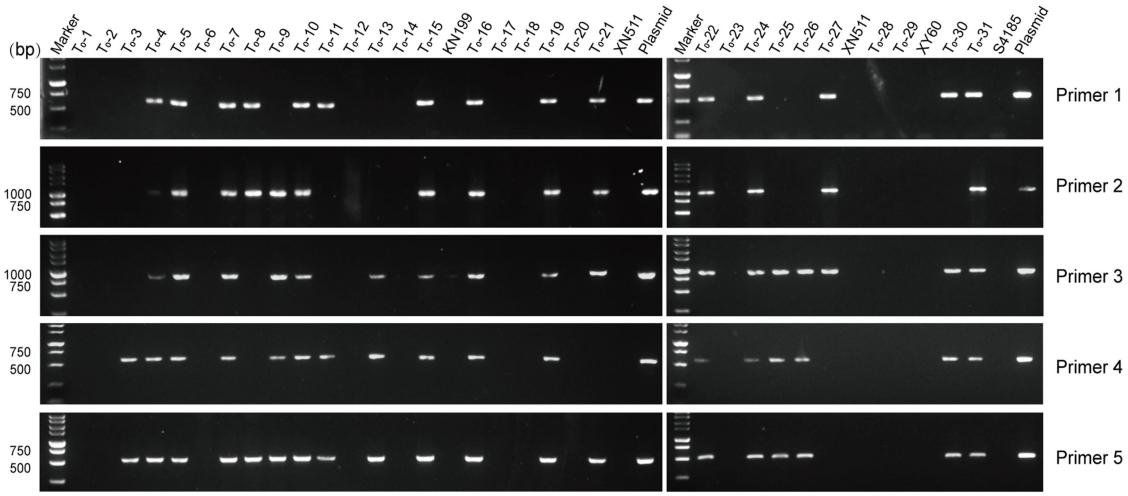

Extended Data Fig. 7 | Detection of transgene-free mutants. Outcome of tests for transgene-free mutants using five primer sets in 31 mutant plants in Extended Data Table 2. Lanes labelled WT and plasmid show the PCR fragments amplified from a WT plant and plasmid constructs pJIT163-Ubi-Cas9 and pU6-gRNA vector respectively. KN-WT, XN-WT, XY-WT and S-WT indicate elite wheat varieties KN199, XN511, XY60 and S4185. Experiments were repeated 3 times with the same results.

Extended Data Table 1 | Frequencies of mutations generated by genome editing with CRISPR-Cas9 DNA/RNP in the T_0 generation of four elite wheat varieties

Wheat variety	Delivery form	No. of bombarded immature embryos	No. of mutants with large deletion/ mutagenesis (%)*	No. of mutants with desired mutation/frequency (%)†
KN199	DNA	1700	15 (0.9)	5 (33.3)
KN199	RNP	550	4 (0.7)	2 (50.0)
XN511	DNA	1300	12 (0.9)	7 (58.3)
S4185	DNA	500	2 (0.4)	2 (100.0)
S4185	RNP	800	3 (0.4)	0 (0)
XY60	DNA	600	2 (0.3)	0 (0)
XY60	RNP	500	1 (0.2)	0 (0)

*On the basis of the number of plants carrying the large deletion in the B genome over the total number of bombarded immature embryos. †On the basis of the number of plants carrying site-specific indels in at least one allele in each *MLO-A1* and *MLO-D1* over the total number of mutant plants with the large deletion in the B genome.

Extended Data Table 2 | Genotypes of the mutants generated by CRISPR-Cas9 DNA in terms of mutations in *TaMLO-A1*, *TaMLO-D1* and the large deletion in the B genome

Genotype of *TaMLO1* homeologs	Plant ID	Mutation detected (bp)[a]	CRISPR-free[b]	Wheat variety	Genotype of *TaMLO1* homeologs	Plant ID	Mutation detected (bp)[a]	CRISPR-free[b]	Wheat variety
AAB^{r}b^{r}DD	T_0-4	dele (*B^{r}b^r*)	NO	KN199	*AAB^{r}b^{r}dd*	T_0-19	dele (*B^{r}b^r*); -35/+86, +91 (*dd*)	NO	XN511
	T_0-5	dele (*B^{r}b^r*)	NO	KN199	*AaB^{r}b^{r}Dd*	T_0-9	V-A (*Aa*); dele (*B^{r}b^r*); H-R (*Dd*)	NO	KN199
	T_0-6	dele (*B^{r}b^r*)	YES	KN199	*Aabb^{r}dd*	T_0-1	-24 (*Aa*); +1, dele (*bb^r*); +1, -3 (*dd*)	YES	KN199
	T_0-11	dele (*B^{r}b^r*)	NO	KN199		T_0-20	+1 (*Aa*); -36, -14, dele (*bb^r*); -35/+86, +90 (*dd*)	YES	XN511
	T_0-14	dele (*B^{r}b^r*)	YES	KN199		T_0-24	-1 (*Aa*); +1, +55, WT, dele (*bb^r*); -9, -69 (*dd*)	NO	XN511
	T_0-15	dele (*B^{r}b^r*)	NO	KN199	*aaB^{r}b^{r}dd*	T_0-25	+1, +1 (*aa*); dele (*B^{r}b^r*); -9, -1 (*dd*)	NO	XN511
	T_0-21	dele (*B^{r}b^r*)	NO	XN511	*aaB^{r}b^{r}Dd*	T_0-31	-9, +1 (*aa*); dele (*B^{r}b^r*); +1, WT (*Dd*)	NO	S4185
	T_0-26	dele (*B^{r}b^r*)	NO	XN511	*aabb^{r}Dd*	T_0-2	-3/+120, -43 (*aa*); -16, dele (*bb^r*); +1 (*Dd*)	YES	KN199
	T_0-27	dele (*B^{r}b^r*)	NO	XN511		T_0-17	+1, -7 (*aa*); -1, dele (*bb^r*); -1 (*Dd*)	YES	XN511
	T_0-29	dele (*B^{r}b^r*)	YES	XY60		T_0-12	-4, +1 (*aa*); -9, WT, dele (*bb^r*); -3 (*Dd*)	YES	KN199
AAbb^{r}DD	T_0-10	-14, -36, WT, dele (*bb^r*)	NO	KN199	*aabb^{r}dd*	T_0-13	+1, -3 (*aa*); +55, dele (*bb^r*); -2, -3 (*dd*)	NO	KN199
AAB^{r}b^{r}Dd	T_0-3	dele (*B^{r}b^r*); H-P (*Dd*)	NO	KN199		T_0-18	-22, -39 (*aa*); +103, +175, dele (*bb^r*); -3/135, +1 (*dd*)	YES	XN511
	T_0-7	dele (*B^{r}b^r*); V-A (*Dd*)	NO	KN199		T_0-22	-14, -21 (*aa*); +1, dele (*bb^r*); +454, +312 (*dd*)	NO	XN511
	T_0-8	dele (*B^{r}b^r*); -1 (*Dd*)	NO	KN199		T_0-23	-15, +1 (*aa*); +1, dele (*bb^r*); +221/-13, +285 (*dd*)	YES	XN511
	T_0-16	dele (*B^{r}b^r*); T-A (*Dd*)	NO	XN511		T_0-30	-43, +1 (*aa*); -9, dele (*bb^r*); +1, -4 (*dd*)	NO	S4185
	T_0-28	dele (*B^{r}b^r*); +1 (*Dd*)	YES	XY60					

[a]"–" indicates deletion of the indicated number of nucleotides; "+" indicates insertion of the indicated number of nucleotides; "–/+" indicates simultaneous deletion and insertion of the indicated numbers of nucleotides at the same site. "*B^r*" indicates the wild-type B genome; "*b^r*" indicates the 304-kb deletion; "*b*" indicates indels in *MLO-B1*. H-P, T-A, V-A and H-R indicate amino acid substitutions. [b]Based on whether mutant plants harbored the CRISPR DNA construct or not.

Extended Data Table 3 | Genotypes of the mutants generated by CRISPR-Cas9 RNP with respect to mutations in *TaMLO-A1*, *TaMLO-D1* and the large deletion in the B genome

Plant ID	Wheat variety	Genotype of *TaMLO1* homeologs	Mutation detected (bp)[a]	Plant ID	Wheat variety	Genotype of *TaMLO1* homeologs	Mutation detected (bp)[a]
T_0-32	XY60	*AAB′b′Dd*	dele (*B′b′*); +1(*Dd*)	T_0-36	KN199	*AAB′b′Dd*	dele (*B′b′*); V-A(*Dd*)
T_0-33	S4185	*AaB′b′DD*	F-S(*Aa*); dele (*B′b′*)	T_0-37	KN199	*AaB′b′DD*	-1(*Aa*); dele (*B′b′*)
T_0-34	S4185	*AAB′b′DD*	dele (*B′b′*)	T_0-38	KN199	*Aabb′Dd*	+1, -3, WT(*Aa*); +1, WT, dele (*bb′*); -6, -7, WT*(Dd*)
T_0-35	S4185	*AAB′b′DD*	dele (*B′b′*)	T_0-39	KN199	*aabb′dd*	-7(*aa*); -4, dele (*bb′*); +1, -5(*dd*)

[a]"–" indicates deletion of the indicated number of nucleotides; "+" indicates insertion of the indicated number of nucleotides; "–/+" indicates simultaneous deletion and insertion of the indicated numbers of nucleotides at the same site. "*B*′" indicates the wild-type B genome; "*b*′" indicates the 304-kb deletion; "*b*" indicates indels in *MLO-B1*. F-S, V-A indicate amino acid substitutions.

nature portfolio

Corresponding author(s): Caixia Gao

Last updated by author(s): Oct 19, 2021

Reporting Summary

Nature Portfolio wishes to improve the reproducibility of the work that we publish. This form provides structure for consistency and transparency in reporting. For further information on Nature Portfolio policies, see our Editorial Policies and the Editorial Policy Checklist.

Statistics

For all statistical analyses, confirm that the following items are present in the figure legend, table legend, main text, or Methods section.

n/a	Confirmed
☐	☒ The exact sample size (*n*) for each experimental group/condition, given as a discrete number and unit of measurement
☐	☒ A statement on whether measurements were taken from distinct samples or whether the same sample was measured repeatedly
☐	☒ The statistical test(s) used AND whether they are one- or two-sided *Only common tests should be described solely by name; describe more complex techniques in the Methods section.*
☒	☐ A description of all covariates tested
☐	☒ A description of any assumptions or corrections, such as tests of normality and adjustment for multiple comparisons
☐	☒ A full description of the statistical parameters including central tendency (e.g. means) or other basic estimates (e.g. regression coefficient) AND variation (e.g. standard deviation) or associated estimates of uncertainty (e.g. confidence intervals)
☐	☒ For null hypothesis testing, the test statistic (e.g. *F*, *t*, *r*) with confidence intervals, effect sizes, degrees of freedom and *P* value noted *Give P values as exact values whenever suitable.*
☒	☐ For Bayesian analysis, information on the choice of priors and Markov chain Monte Carlo settings
☒	☐ For hierarchical and complex designs, identification of the appropriate level for tests and full reporting of outcomes
☒	☐ Estimates of effect sizes (e.g. Cohen's *d*, Pearson's *r*), indicating how they were calculated

Our web collection on statistics for biologists contains articles on many of the points above.

Software and code

Policy information about availability of computer code

Data collection	Illumina NovaSeq platform was used to collect the amplicon deep sequencing data; Olympus BX51 light microscope with Cellsens Entry 1.21 software; SPAD-502 Minolta; Bio-Rad CFX96 with CFX Maestro 1.1 software; Bio-rad Universal Hood II- GelDoc System with Image Lab v5.2 software; Nikon D90 camera
Data analysis	Graphpad prism 8.0.1 was used to analyze the data. All NGS data were analyzed as previously described. For RNA-seq data analysis, fastp (version 0.20.1), hisat2 (version 2.1.0), FeatureCount (version 1.6.4) and edgeR (version 3.32.1) were used. For 4C-seq data analysis, pipe4C (https://github.com/deLaatLab/pipe4C) was used. For CUT&Tag and ATAC-seq data analysis, fastp (version 0.20.1), BWA mem algorithm (version 0.7.15-r1140), Samtools (version 1.9), Picard (version 2.26.3), MACS2 (version 2.1.2), DeepTools (version 3.5.0) and IGV (version 2.8.13) were used.

For manuscripts utilizing custom algorithms or software that are central to the research but not yet described in published literature, software must be made available to editors and reviewers. We strongly encourage code deposition in a community repository (e.g. GitHub). See the Nature Portfolio guidelines for submitting code & software for further information.

Data

Policy information about availability of data

All manuscripts must include a data availability statement. This statement should provide the following information, where applicable:

- Accession codes, unique identifiers, or web links for publicly available datasets
- A description of any restrictions on data availability
- For clinical datasets or third party data, please ensure that the statement adheres to our policy

The authors declare that all data supporting the findings of this study are available in the article and its Supplementary Information files. Source data are provided

with this article. Datasets of all next generation sequencing have been deposited and made available in the Genome Sequence Archive (GSA) database in BIG Data Center (https://ngdc.cncb.ac.cn/) under accession Number PRJCA005687; Chinese Spring wheat reference genome RefSeq v1.1 is available on IWGSC (http://www.wheatgenome.org/); Transcriptome data of wheat different tissues are from previous publication (DOI: 10.1126/science.aar6089)

Field-specific reporting

Please select the one below that is the best fit for your research. If you are not sure, read the appropriate sections before making your selection.

☒ Life sciences ☐ Behavioural & social sciences ☐ Ecological, evolutionary & environmental sciences

For a reference copy of the document with all sections, see nature.com/documents/nr-reporting-summary-flat.pdf

Life sciences study design

All studies must disclose on these points even when the disclosure is negative.

Sample size	The sample size and the results of statistical analyses are described in the relevant figures or method section. Sample size was determined based on experimental trials to allow for confident statistical analyses.
Data exclusions	No data that pass quality control were exclusion from analysis.
Replication	All experiments were replicated at least 3 times. Results were reproducible in all repeats with the same trend.
Randomization	Plants were allocated with different genotypes and were grown side by side to minimize unexpected environmental variations during growth and experimentation. Plants for measurement in each group were collected randomly from the population.
Blinding	The investigators were not blinded to group allocation during experiment. The research materials are plants so the blinding design is not applicable, as different plant genotypes may show different morphology, making blinding impossible. Samples were collected randomly or repeat experiment for at least three times with similar trend. Experiments were conducted based on routine practice and were repeated by different authors. Some cases processed automated procedures (DNA sequencing, transformation) that should not bias outcomes.

Reporting for specific materials, systems and methods

We require information from authors about some types of materials, experimental systems and methods used in many studies. Here, indicate whether each material, system or method listed is relevant to your study. If you are not sure if a list item applies to your research, read the appropriate section before selecting a response.

Materials & experimental systems

n/a	Involved in the study
☐	☒ Antibodies
☒	☐ Eukaryotic cell lines
☒	☐ Palaeontology and archaeology
☒	☐ Animals and other organisms
☒	☐ Human research participants
☒	☐ Clinical data
☒	☐ Dual use research of concern

Methods

n/a	Involved in the study
☒	☐ ChIP-seq
☒	☐ Flow cytometry
☒	☐ MRI-based neuroimaging

Antibodies

Antibodies used	Anti-H3K36me3(Abcam,Cat# ab9050, 1/50 dilution), Anti-H3K27ac antibody(Abcam, Cat#ab4729, 1/50 dilution), Anti-H3K4me3 antibody (Abcam, Cat#ab8580, 1/50 dilution), Anti-H3K27me3 antibody (Abcam, Cat#ab6002, 1/50 dilution), Guinea Pig anti-Rabbit IgG (Heavy & Light Chain) antibody (Antibodies-Online company, Cat#ABIN101961, 1/100 dilution), Anti-RNA polymerase II CTD (phospho S5) (Abcam, Cat#ab5408, 1/100 dilution)
Validation	All primary antibodies are commercially available. All validation statements can be found on the manufacturers' websites (Antibodies-Online:https://www.antibodies-online.com/antibody; Abcam, https://www.abcam.com/nav/primary-antibodies).